Earthquakes generated from bedding plane-parallel reverse faults above an active wedge thrust, Seattle fault zone

Harvey M. Kelsey
Department of Geology, Humboldt State University, Arcata, California 95521, USA

Brian L. Sherrod
U.S. Geological Survey, Earth and Space Sciences, University of Washington, Seattle, Washington 98193-1310, USA

Alan R. Nelson
U.S. Geological Survey, MS 966, Box 25046, Denver, Colorado 80225-0046, USA

Thomas M. Brocher
U.S. Geological Survey, 345 Middlefield Road, MS 977, Menlo Park, California 94025, USA

ABSTRACT

A key question in earthquake hazard analysis is whether individual faults within fault zones represent independent seismic sources. For the Seattle fault zone, an upper plate structure within the Cascadia convergent margin, evaluating seismic hazard requires understanding how north-side-up, bedding-plane reverse faults, which generate late Holocene fault scarps, interact with the north-vergent master-ramp thrust and overlying backthrust of the fault zone. A regional uplift at A.D. 900–930 involved an earthquake that nucleated at depth and included slip on both the master-ramp thrust and the backthrust. This earthquake also included slip on some of the <6-km-deep north-side-up, bedding-plane reverse faults. At locales where the north-side-up reverse faults intersect the Puget Sound coast, an earthquake a few centuries earlier than the A.D. 900–930 regional uplift only uplifted areas within hundreds of meters north of the reverse faults. We infer that the bedding-plane reverse faults are seismogenic because shore platforms near the reverse faults have been abruptly uplifted during earthquakes when other shorelines in the Seattle fault zone were unaffected. Faults of the Seattle fault zone therefore can both produce regional uplift earthquakes, with or without surface displacement on the reverse faults, and produce earthquakes that rupture the bedding-plane reverse faults causing fault scarps and uplift localized to hundreds of meters north of these faults. This latter type of earthquake has occurred at least twice and perhaps three times in the late Holocene, and all these earthquakes preceded the regional coseismic uplift of A.D. 900–930. To account for the paleoseismic observations, we propose that the Seattle fault zone is a wedge thrust, with the leading edge being a fault-bend, wedge thrust fold. The active axial surface of the wedge thrust fold is pinned at the tip of the wedge, and a steeply north-dipping sequence of Tertiary sediment forms the south limb of the wedge thrust fold. Some of these steeply north-dipping, bedding-plane surfaces are seismogenic reverse faults that produce scarps. Earthquakes on the wedge thrust produce the regional coseismic uplift events, and earthquakes within the fault-bend fold cause the local uplift earthquakes. Thus, bedding-plane faults can rupture during earthquakes when the wedge thrust does not rupture but instead continues to accumulate seismic energy.

Keywords: reverse faults, fault-bend folds, Seattle fault zone, paleoseismology, relative sea level.

INTRODUCTION

Seattle Fault Zone

Active faults on master-ramp thrusts that do not reach the surface (blind faults) pose a serious but hidden earthquake hazard (Stein and King, 1984; Yeats, 1986). Folds related to such faults often are manifest at the surface (Wentworth and Zoback, 1990; Stein and Ekström, 1992; Guzofski et al., 2007) or in near-surface boreholes (Dolan et al., 2003), and such folds aid in describing the character (recurrence interval, magnitude, and coseismic slip amounts) of blind, master-ramp earthquakes. Blind faults pose another potential seismic hazard through coseismic folding (Chen et al., 2007). Most studies ascribe fold growth associated with master-ramp earthquakes to slip on the master ramp (Wentworth and Zoback, 1990; Stein and King, 1984); however, another seismic hazard comes from fold growth during discrete and separate earthquakes not associated with direct motion on the master ramp. In this paper we make the case that, in addition to the seismic hazard from earthquakes on a blind master-ramp thrust, the Seattle fault zone poses an independent seismic hazard from coseismic folding of fault-bend folds above the master ramp.

The Seattle fault zone is an upper crustal fault zone in the upper plate of the Cascadia convergent margin (Bucknam et al., 1992; Johnson et al., 1999). An east-trending deformation zone, the Seattle fault zone (Fig. 1A) accommodates north-south contraction (Wells et al., 1998; McCaffrey et al., 2000). The zone is defined by the south edge of the Seattle basin and the north edge of the Seattle uplift, a transition that is clearly defined on seismic reflection profiles (ten Brink et al., 2002; Brocher et al., 2004) (Fig. 2B). Surface manifestations of the Seattle fault zone consist of three structural elements. First, bedding within Oligocene and Miocene sedimentary strata is steeply dipping to the north (Fulmer, 1975; McLean, 1977) (Figs. 1B and 2A) within a monoclinal fold that separates rocks of the Eocene Crescent volcanic basement that are at or near the surface south of the Seattle monocline (hachured zone, Fig. 1A) from flat-lying Quaternary sediments of the Seattle basin

†E-mail: hmk1@humboldt.edu

GSA Bulletin; November/December 2008; v. 120; no. 11/12; p. 1581–1597; doi: 10.1130/B26282.1; 11 figures.

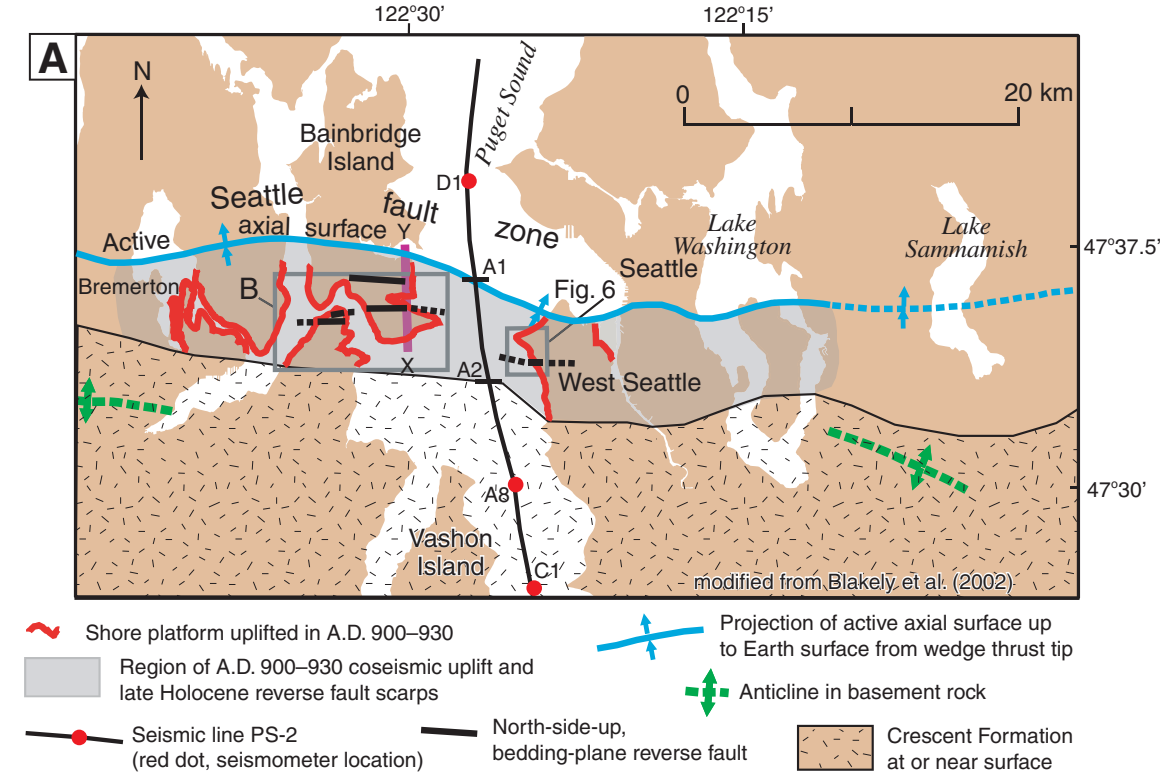

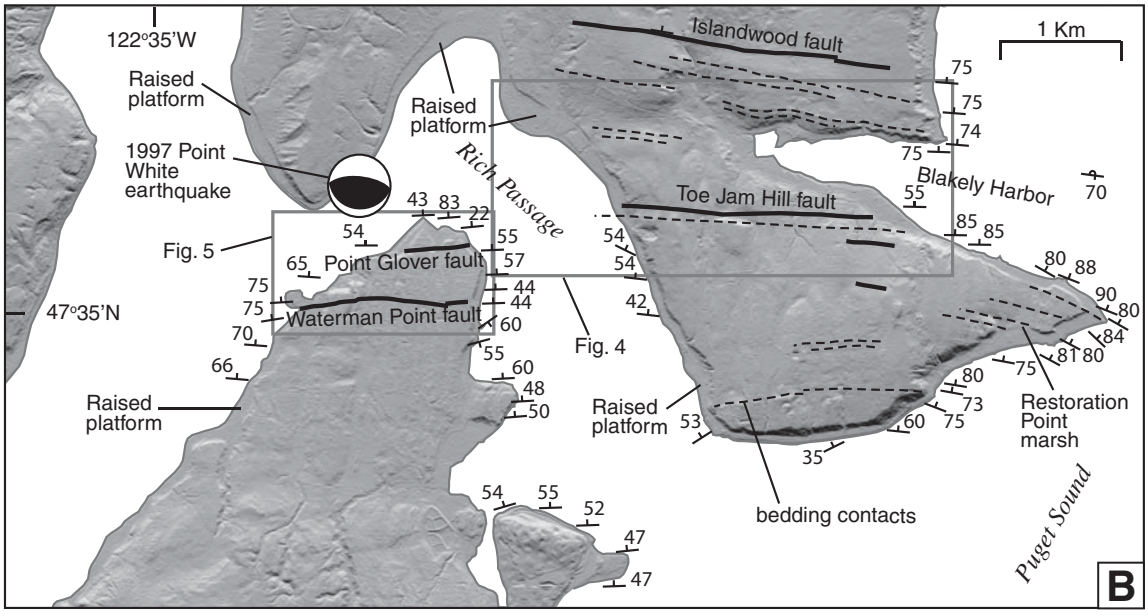

Figure 1. (A) Map of Seattle fault zone modified from Blakely et al. (2002). (B) Light detection and ranging (LiDAR) image of southern Bainbridge Island and Waterman Point-Point Glover Peninsula, showing the trace of the Toe Jam Hill, Islandwood, Waterman Point and Point Glover faults. The coastline is fringed by a wave-cut platform that emerged ~1100 yr ago (Bucknam et al., 1992). The platform exposes tilted strata of the Miocene Blakely Harbor and Eocene Blakeley formations. Strike and dip measurements from Fulmer (1975) and McLean (1977).

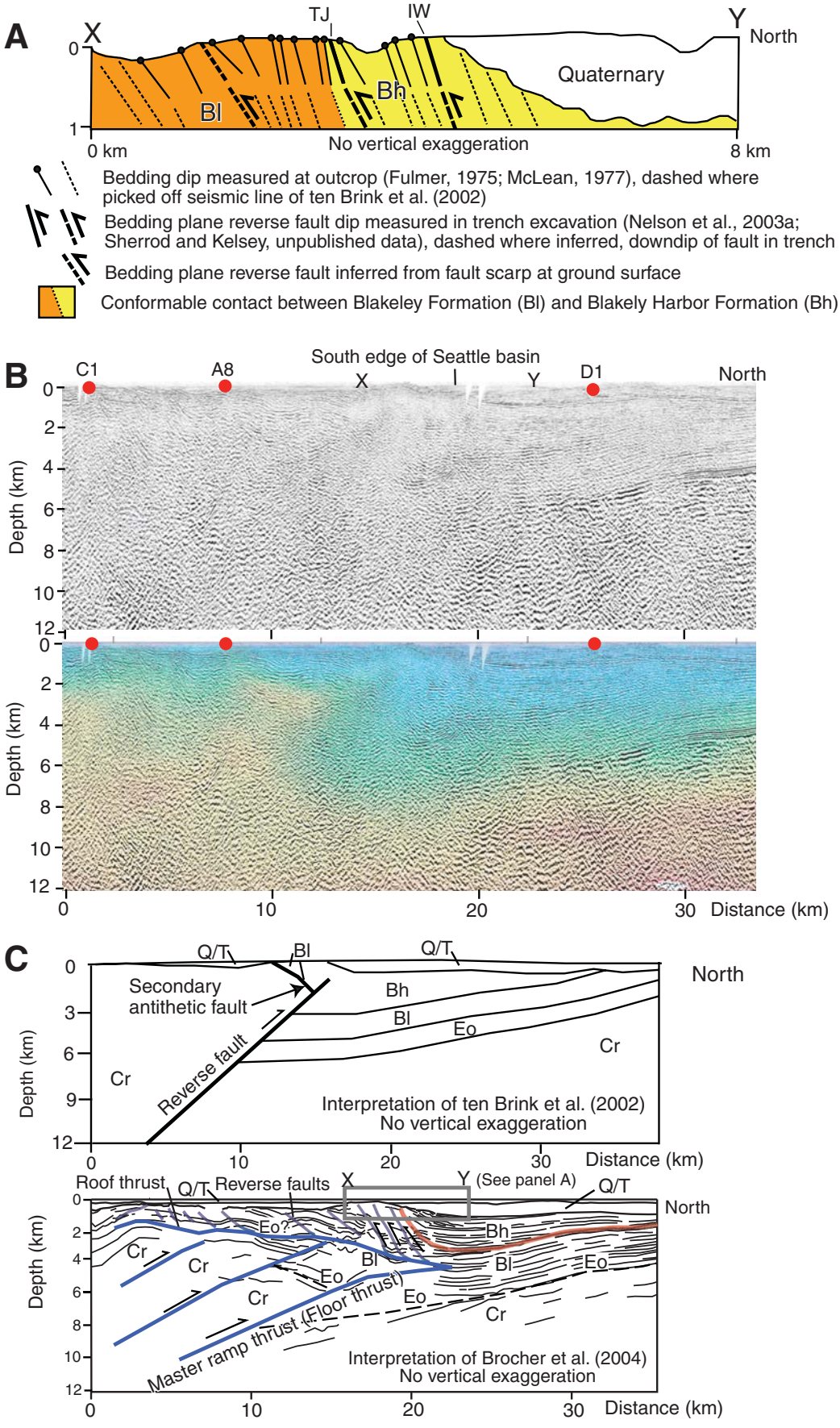

Figure 2. (A) Cross section showing observed dips of bedding on south end of Bainbridge Island (cross section located on Fig. 1). Bedding-plane reverse faults observed in trench excavations (TJ—Toe Jam Hill fault, IW—Islandwood fault) are depicted. Subsurface dips of faults and bedding are reflectors on seismic line PS-2 (ten Brink et al., 2002). (B) Seismic Hazards Investigation in Puget Sound (SHIPS) seismic reflection line PS-2 (black and white) and coincident P-wave–velocity model (color) (ten Brink et al., 2002). C1, A8, and D1 are locations of seismometers along seismic line (Fig. 1A). (C) Two previously published interpretations of the structure of the Seattle fault zone (ten Brink et al., 2002; Brocher et al., 2004), both based on seismic profile line PS-2 and in part in conjunction with oil industry seismic reflection lines (Brocher et al., 2004). This paper discusses an alternative interpretation (Fig. 9). Cr—Eocene Crescent Formation basalt; Eo—Eocene sediment; Bl—Blakeley Formation; Bh—Blakely Harbor Formation; Q/T—Quaternary and late Tertiary (post–Miocene) sediment.

north of the monocline (Figs. 1A and 2B). Second, within the Seattle fault zone there is an east-trending, ~6- to 7-km–wide zone that was regionally uplifted by ~5–7 m ~1100 yr ago (Bucknam et al., 1992), and this uplifted zone is delineated by a raised shore platform (red area, Fig. 1A). The uplifted zone is of limited north-to-south width because of the increasing depth, to the south, of the master-ramp fault that drives surface uplift (ten Brink et al., 2006.) Third, the Seattle fault zone is characterized by reverse faults with late Holocene fault scarps (Nelson et al., 2003a, 2003b, 2003c) (black lines, Fig. 1A), east trending and up to the north, that are of limited individual segment lengths (0.5–5 km) but are overlapping and as a system extend at least 16 km east-west along the fault zone (Fig. 1A).

Geophysical imaging of the Seattle fault zone, when considered with the fault zone characteristics discussed above, yields an integrated structural view of the Seattle fault zone. Aeromagnetic anomalies clearly delineate east-trending structural discontinuities along the zone (Blakely et al., 2002). Based on previous interpretations of seismic reflection data (Pratt et al., 1997; ten Brink et al., 2002; Brocher et al., 2004) (Fig. 2), the Seattle fault zone consists of a south-dipping, blind master-ramp thrust or master reverse fault at intermediate (7–10 km) to shallow (5–7 km) crustal levels (Fig. 2C). Structural interpretations at shallower levels are variable, as discussed below.

Although the Seattle fault zone is east trending, the fault zone only shows evidence of Holocene surface deformation between the vicinity of Bremerton on the west and the east shore of Lake Washington on the east, an along-strike distance of ~40 km (Fig. 1A). Portraying the overall neotectonic framework of the Seattle fault zone, which is beyond the scope of this study, will require better definition of the active extent of the fault to the east and to the west.

Paleoseismic History of the Seattle Fault Zone from Raised Shorelines, Trench Excavations, and Marsh Stratigraphy

Scrutiny of both late Holocene raised shorelines and east-trending, up-to-the-north fault scarps by recent investigators has resulted in a paleoseismic history of the Seattle fault zone. Bucknam et al. (1992) first recognized multiple meters of abrupt uplift from late Holocene shore platforms straddling the Seattle uplift, and inferred the uplift to be recent in age (1100 yr ago), regional in extent (Fig. 1A), and earthquake caused. Atwater (1999) refined the age of the most recent, regional uplift event on the Seattle fault to be ~1100 yr ago (A.D. 900–930) based on debris deposited by a tsunami triggered by an 1100 yr ago earthquake (Atwater and Moore, 1992). Sherrod et al. (2000) used a 7500-yr continuous relative sea level record from Restoration Point marsh on Bainbridge Island (Fig. 1B) to conclude that the A.D. 900–930 regional uplift within the Seattle fault zone was the only one in the past 7000 yr.

Using airborne light detection and ranging (LiDAR) images, several late Holocene fault scarps were discovered in the Puget lowland (Harding, 2002; Haugerud et al., 2003), and subsequent trenching investigations revealed that the scarps delineate steeply dipping, north-side-up reverse faults that slip along bedding planes of the Oligocene Blakeley Formation and the Miocene Blakely Harbor Formation (Nelson et al., 2003a, 2003b, 2003c). The north-side-up reverse faults on Bainbridge Island slipped during at least four earthquakes in the late Quaternary, with the three most recent earthquakes in the past ~3000 yr (Nelson et al., 2003a).

Bedding-Plane Reverse Faults and Structural Model of the Seattle Fault Zone

Bedding-plane reverse faults are an important structural element at the uppermost structural level of the Seattle fault zone because such faults form all the late Quaternary scarps. The steeply dipping beds at the surface (60°–80°), which define the north-dipping panel of the monocline, align with steeply dipping reflectors in the subsurface on seismic lines (Fig. 2A).

Two conceptual models—a reverse fault with secondary antithetic fault model (ten Brink et al., 2002) and a floor thrust-roof thrust duplex model (Brocher et al., 2004) (Fig. 2C)—can account for the broad uplift (~6–7 km width) along the Seattle fault zone by slip on a master-ramp thrust and a backthrust or "roof ramp" (ten Brink et al., 2006). In a structural duplex, reverse faults cut up from a lower basal detachment and merge at a higher stratigraphic level to form another detachment, called a roof thrust (Marshak and Mitra, 1988). Brocher et al. (2004) suggested that the Seattle fault zone is a passive roof duplex with the shallow (<5 km depth) reverse faults (purple faults, Fig. 2C) being passive (nonseismogenic) splay faults off a south-vergent roof thrust. The roof thrust model of Brocher et al. (2004) can account for the observed north-side-up reverse faults and can accommodate simultaneous coseismic shortening on a north-vergent thrust fault at depth and on secondary south-vergent (north-side-up) reverse faults at the surface. In contrast, an alternative model consisting of a reverse fault with a secondary antithetic thrust (ten Brink et al., 2002) (Fig. 2C) cannot accommodate the location or movement history of the north-side up-reverse faults (ten Brink et al., 2006).

The floor thrust-roof thrust duplex model of Brocher et al. (2004) (Fig. 2C) is a starting point to evaluate earthquake sources on the Seattle fault zone. Inherent in the floor thrust-roof thrust duplex model is the assumption that the bedding-plane reverse faults that splay off the roof thrust are passive and not seismogenic. However, faults that occur on bedding-plane surfaces in bedded sedimentary rocks may be seismogenic. For instance, in the offshore Santa Barbara Channel in southern California, Shaw and Suppe (1994) described seismicity that they inferred records folding of fault-bend folds by bedding-plane slip. The hypocentral locations of earthquakes from a 1984 M_L 0.5–4.0 swarm define a steeply dipping plane at the location of an axial surface mapped from well logs. Focal mechanism solutions for some of the earthquakes (Henyey and Teng, 1985) were consistent with folding by bedding-plane slip in the vicinity of the axial surface but were also consistent with a high-angle fault cutting across bedding. More recent work interprets the axial surface of the fault-bend fold also to be a high-angle fault (Nicholson et al., 2007). In the case of the 1984 Santa Barbara Channel seismicity, the swarm of earthquakes that Shaw and Suppe (1994) associated with folding was not accompanied by coseismic slip on an underlying master ramp. Therefore, Shaw and Suppe (1994) inferred that bedding-plane flexural slip associated with a fault-bend fold can be an independent seismic source. Whether or not Shaw and Suppe's (1994) interpretation is correct for a particular structure in the Santa Barbara channel, their conceptual contribution, that bedding-plane flexural slip associated with a fault-bend fold can be an independent seismic source, is significant. Similarly, our data on deformation of bedding-plane reverse faults that offset wave-cut platforms on the Seattle uplift suggest that these faults are not passive and represent potential independent seismic sources.

Research Questions

We use uplifted shoreline data to investigate whether the upper structural levels of the Seattle fault zone are passive, as initially proposed, or active earthquake sources. Our evaluation of the structural model of the Seattle fault zone is prompted by three questions. First, if all Seattle fault zone earthquakes involve rupture of the master ramp (the "floor thrust" of Brocher et al., 2004), which then impels a coseismic regional uplift along the Seattle fault zone, then why is there only one regional uplift in the late Holocene (implying just one late Holocene earthquake)

when there is evidence in trenches excavated across reverse faults of the Seattle fault zone for multiple late Holocene earthquakes?

Second, are the north-side-up, bedding-plane reverse faults that trend through the Seattle urban area seismic sources for earthquakes? Such earthquakes would be smaller in magnitude than the earthquakes with source foci on the master-ramp thrust because they would involve less fault rupture area than earthquakes on the master ramp, but they also would be shallower (~5 km versus ~12 km) and could pose a seismic hazard to the Seattle metropolitan area.

Third, if the north-side-up reverse faults produce earthquakes, then there should be uplifted shore platforms of limited areal extent that are a distinct product of these earthquakes. Do such uplifted shore platforms, limited in extent and not correlative to the regionally uplifted A.D. 900–930 platform, exist? What is the likely rupture area and magnitude of such earthquakes given the areal extent, fault scarp length, and amounts of fault displacement on these raised shore platforms?

RESEARCH APPROACH

Shoreline Angles as Paleogeodetic Benchmarks

The best measure of the amount of vertical displacement between a modern shore platform and a raised platform is a comparison of the elevation of the modern shoreline angle to the elevation of the shoreline angle of the raised platform (Hull, 1987). The shoreline angle is the intersection of the inner edge of the modern shore platform with the base of the modern sea cliff (Fig. 3; gray squares on profile lines, Figs. 4 and 5). Uplifted shoreline angles are buried by colluvium from the paleo–sea cliff, and their elevations are determined by digging holes in the uplifted terrace seaward of the colluvial covered shoreline angle, identifying the platform (wave-cut strath) in the subsurface and then projecting the strath shoreward to the base of the paleo–sea cliff.

Shoreline angle elevations, determined by leveling, were tied to a tidal benchmark through surveying low tides. The accuracy of the elevations is ~1 m, limiting our investigation to earthquakes uplifting the platform by more than this amount. Elevation uncertainty depends on four controlling variables: surveying uncertainty (5 mm, based on the upper limit to survey closures from multiple survey loops), inherent relief of the strath surface (relief of the modern strath surface averages 0.25 m; relief can be as large as one meter but over most of the exposed modern strath relief is ~0.25 m), accuracy of identifying the strath in soil pits (accurate within 10 mm based on observations in pit excavations), and accuracy of projecting the strath surface landward to the paleo–sea cliff (an extrapolation procedure with uncertainty up to 1.0 m). The uncertainty in determining paleoshoreline angle elevation, approximated by taking the square root of the sum of the squares of the uncertainties, is ~1 m. The uncertainty in projecting the strath surface landward to the paleo–sea cliff dominates all other uncertainties.

Shore Platform Investigations

We utilized deformed shore platforms that intersect north-side-up reverse fault scarps at three coastal sites to determine if shorelines were deformed in the late Holocene at times other than during the A.D. 900–930 regional uplift earthquake. We determined vertical displacement on north-side-up reverse faults by differencing shoreline angle elevations for correlated platforms on either side of the fault, and we quantified platform uplift as the elevation difference of modern and uplifted shoreline angles. We assumed that raised late Holocene shore platforms are uplifted during earthquakes because, in the last few thousand years, coseismic vertical displacement is the only way to suddenly lower relative sea level by several meters (Bucknam et al., 1992).

In the zone of the Seattle uplift, coseismic vertical displacement can be a product of either regional uplift (across the ~6- to 7-km–wide "Seattle uplift," gray shaded area in Fig. 1A), local uplift on the upthrown side of reverse faults (uplift confined to hundreds of meters immediately north of reverse fault scarps), or both. Distinctive raised platform geometries are produced by different sequences of regional uplift versus local uplift on reverse faults (Fig. 3).

Of the seven alternative shore platform geometries illustrated in Figure 3, four typify the variation seen in shore platforms at sites intersected by reverse faults. The first shore platform geometry, generated by one earthquake with regional uplift in which the reverse fault did not move (Fig. 3A), occurs where the Toe Jam Hill fault intersects the east coast of Bainbridge Island (Fig. 4). The second shore platform geometry, generated by both regional uplift and reverse fault movement during a single earthquake (Fig. 3B), occurs at the westernmost on-land exposure of the Waterman Point fault (Nelson et al., 2003b) (Fig. 5). The third shore platform geometry, generated first by a reverse fault earthquake and later by a regional uplift earthquake (Fig. 3E), occurs at two sites: where the Toe Jam Hill fault intersects the west coast of Bainbridge Island (Fig. 4) and at Point Glover where the Point Glover fault intersects the coast (Fig. 5). The fourth shore platform geometry, generated first by a reverse fault earthquake and later by both regional uplift and reverse fault movement during one earthquake (Fig. 3G), occurs south of Alki Point, Seattle, where the West Seattle fault intersects the shore of Puget Sound (Fig. 6). Because only the latter three sites implicate two earthquakes separated in time, these three sites were selected for detailed investigation.

SHORE PLATFORM DEFORMATION

West Coast of Bainbridge Island

On the west coast of southern Bainbridge Island, there are two uplifted shore platforms north of the Toe Jam Hill fault and one south of the fault. The shoreline angle of the lowest uplifted platform north and south of the fault (the A.D. 900–930 uplifted platform), where it intersects the west coast, is at the same elevation within the ~1 m survey accuracy (6.3 m versus 5.7 m) (Fig. 4). The elevation of the shoreline angle of the upper platform is 9.0 ± 1.0 m, which is the cumulative uplift from an older earthquake that uplifted the platform for an ~400 m coastwise extent north of the fault, but not south of the fault, and a younger earthquake that regionally uplifted the lower platform; uplift solely from the older earthquake was ~3–3.5 m (9 m minus 5.7 m, Fig. 4). Therefore, on the west coast of Bainbridge Island, there is evidence for two earthquakes in the late Holocene, an earlier earthquake that locally uplifted the platform north of the fault but was not associated with a regional uplift of the Seattle uplift and a younger earthquake that regionally uplifted the coast-fringing shore platforms within the Seattle uplift (case E, Fig. 3).

Coastal evidence for earthquakes in the late Holocene is consistent with paleoseismic data from trenches across the Toe Jam Hill fault scarp. The Toe Jam Hill fault forms a scarp that trends east-west across the southern part of Bainbridge Island, and the scarp dies out as it approaches both the west and east coasts (Fig. 4). Based on three of five trenches dug in the sandstone and shale of the Miocene Blakely Harbor Formation, the fault is a steeply dipping reverse fault that slips along bedding planes (Nelson et al., 2003a). Based on deformed strata in one of the trenches (trench CL, Fig. 4), three earthquakes have occurred on Toe Jam Hill fault after 2.5 ka, and the most recent earthquake of ca. 1.1 ka involved ~2 m of vertical offset of the ground surface caused by slip along 60° to 80° north-dipping bedding contacts of the Miocene Blakely Harbor Formation (Nelson et al., 2003a).

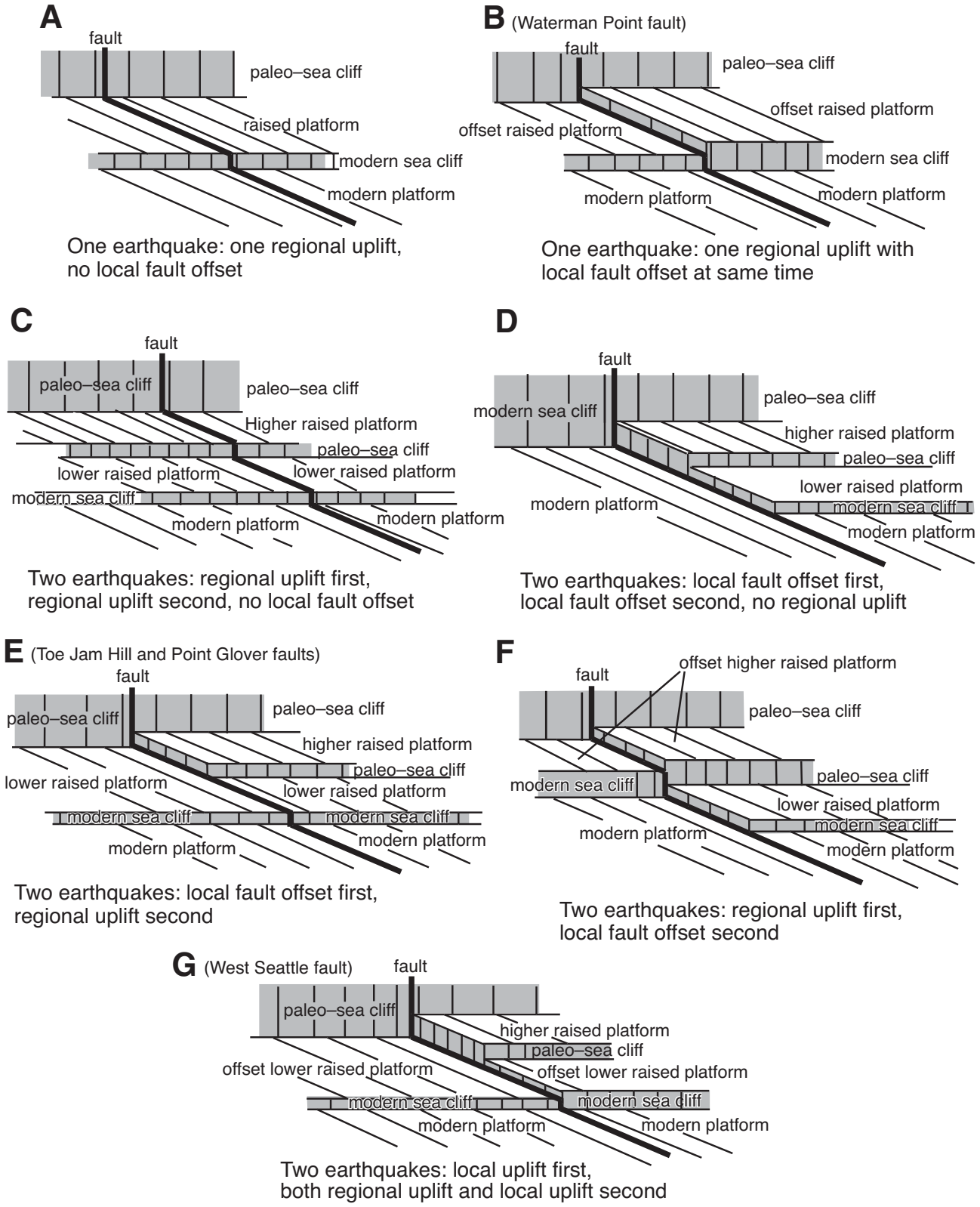

Figure 3. Seven block diagrams showing shore platform geometries for different combinations of one or two earthquakes and regional uplift versus local uplift on one side of a vertical fault. Block diagrams are schematic in that terrace cover sediment is not shown, and the faults are depicted as vertical, whereas the actual faults are steeply dipping reverse faults.

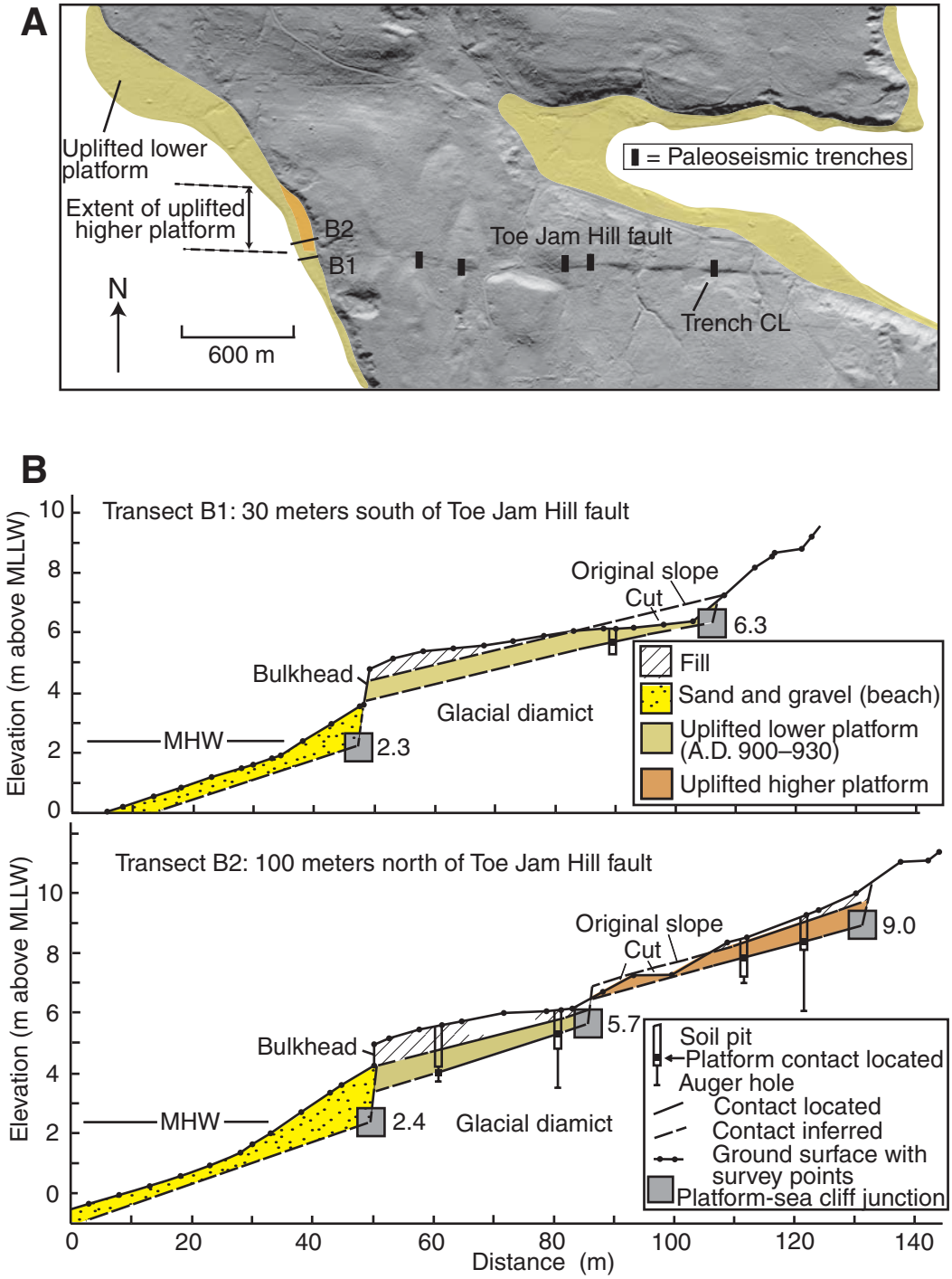

Figure 4. (A) Light detection and ranging (LiDAR) image of a portion of southern Bainbridge Island peninsula (map location on Fig. 1B) showing the scarp of the Toe Jam Hill fault, location of trenches across the fault scarp, and locations of coastal transects depicted at west end of fault trace. Green shade indicates area of the A.D. 900–930 regionally uplifted platform, and orange area on west coast indicates area inferred to have been uplifted during a local earthquake on the Toe Jam Hill fault that preceded the regional uplift earthquake. (B) Two coastal transects near the west end of Toe Jam Hill fault, transect B1 is 30 m south of the fault trace and shows one uplifted shore platform; transect B2 is 100 m north of the fault trace and shows two uplifted shore platforms. Platform elevations are located in soil pit or auger holes to nearest 10 mm. MHW—Mean high water; MLLW—mean lower low water.

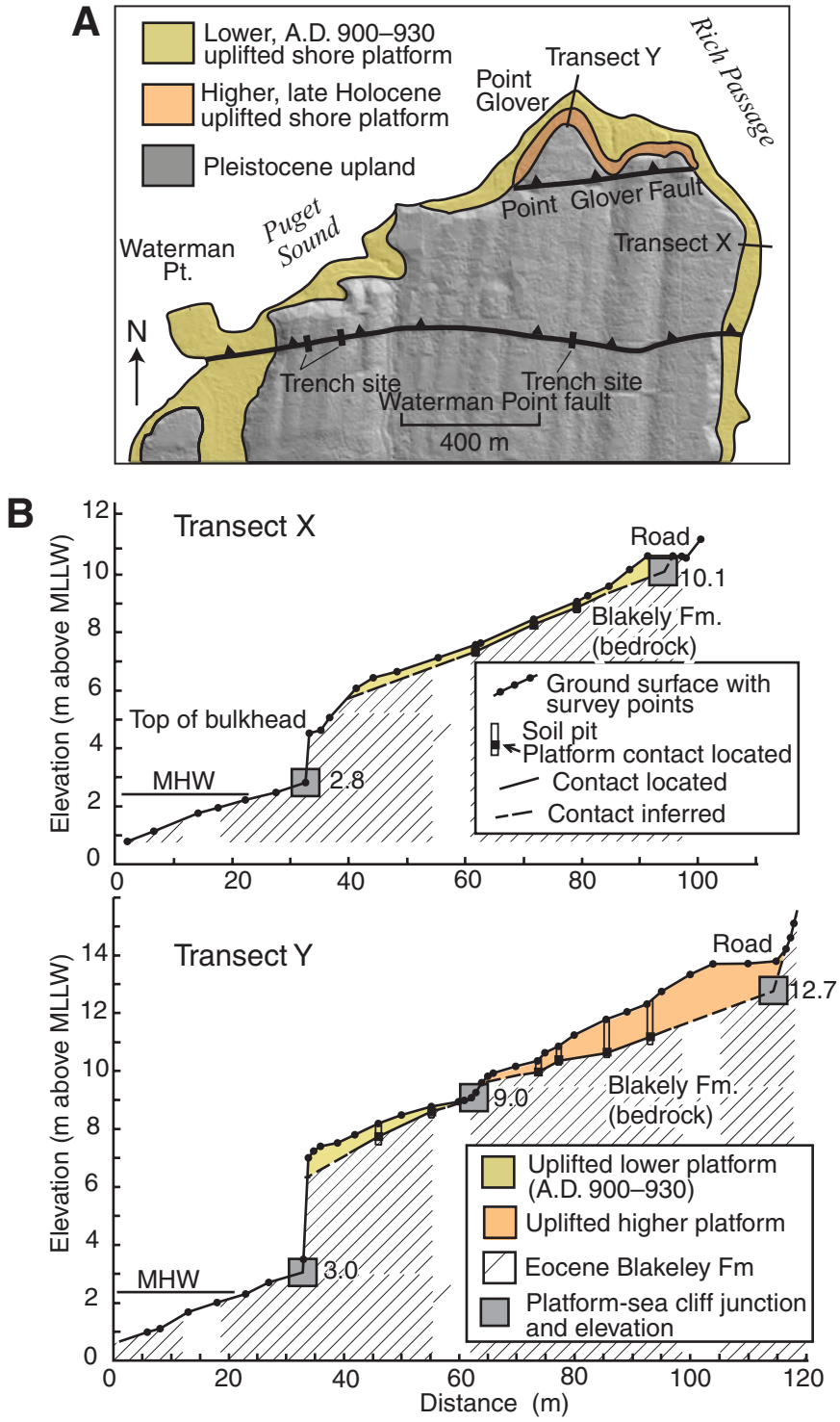

Figure 5. (A) Simplified geologic map of the Point Glover area (map location on Fig. 1B), superposed on light detection and ranging (LiDAR) base, showing the Point Glover and Waterman Point faults, sites of trenches across scarps on the Waterman Point fault, and the higher and older shore platform that is preserved only north of the Point Glover fault. (B) Surveyed, annotated geologic cross sections; transect X is south of the Point Glover fault and shows the elevation of the one uplifted platform and the thickness and extent of paleobeach deposits (green shade). Transect Y is north of the Point Glover fault and shows the elevation of the two uplifted platforms and the thickness and extent of lower and higher paleobeach deposits (green and orange shades, respectively). Platform elevations are located in soil pits to nearest 10 mm. MHW—Mean high water; MLLW—mean lower low water.

Point Glover

There are two uplifted platforms on Point Glover north of the Point Glover fault but only one regionally uplifted platform south of the fault (Fig. 5). The lower platform, which was regionally uplifted during the A.D. 900–930 earthquake (Nelson et al., 2003b, 2003c), extends across the Point Glover fault with no offset (within the 1 m survey resolution). The lower platform maintains the same shoreline angle elevation (9.0 ± 1.0 m) along the 0.75 km coastal extent of the headland. The upper platform only occurs north of the Point Glover fault, and its shoreline angle elevation is 12.7 ± 1.0 m, which is the cumulative uplift from an older earthquake that uplifted the platform just north of the fault, and a younger earthquake that regionally uplifted the lower platform (case E, Fig. 3). Uplift at Point Glover just from the older earthquake was ~3.5–4 m (12.7 minus 9.0 m, Fig. 5).

Similar to Bainbridge Island, therefore, there is evidence for two late Holocene earthquakes at Point Glover. The Point Glover fault slipped during the older earthquake. The 3.5–4.0 m of localized uplift extends at least 200 m north of the fault to where the older platform is eroded by the younger platform. The localized uplift was accommodated by bedding-plane fault slip; and at Point Glover, beds of the Blakely Formation dip ~60° north. The younger earthquake regionally uplifted the lower shore platform by 9.0 ± 1.0 m but did not involve surface rupture of the Point Glover fault.

West Seattle Fault near Alki Point

The extensive A.D. 900–930 uplifted shore platform at West Seattle is offset by the West Seattle fault, an east-trending, north-side-up reverse fault near Alki Point (Fig. 6). Based on auger hole exploration of the depth of the shore platform, the West Seattle fault has offset the A.D. 900–930 platform by ~1.5 m (Fig. 6). Therefore at this site, the regional-uplift earthquake, which involved slip on the north-vergent master ramp at depth (>6 km) (Fig. 2), also involved slip on the south-vergent West Seattle fault at the surface.

A locally higher terrace, which extends ~300 m north of the West Seattle fault and is ~5 m higher than the regionally uplifted shore platform, cannot be explained by only 1.5 m of up-to-the-north offset of the lower platform. We infer that this terrace is evidence for an older, higher shore platform only present immediately north of the West Seattle fault. However, we cannot determine the elevation of the higher platform because both extensive urbanization of

the higher terrace and landsliding of its paleo-sea cliff to the east prevent augering through the cover sediment.

At the highly urbanized West Seattle site, the same late Holocene north-side-up fault that offset the A.D. 900–930 platform apparently is responsible for localized uplift of an older shore platform just north of the fault, a relation similar to two much better exposed and less urbanized faulted shore platform sites on the west coast of Bainbridge Island and at Point Glover. We infer that two earthquakes may be recorded at West Seattle as well. During the earlier earthquake, slip on the West Seattle fault locally elevated a shore platform only north of the fault and a later earthquake regionally uplifted a younger shore platform and again ruptured the West Seattle fault (case G, Fig. 3).

LATE HOLOCENE EARTHQUAKE SCENARIOS ON THE SEATTLE FAULT ZONE

The Toe Jam Hill fault provides the best data set to reconstruct late Holocene earthquake history on the Seattle fault zone because data include both paleoseismic history from exploratory trenches (Nelson et al., 2003a) and paleoseismic history from uplifted shoreline angles (Figs. 4, 5, and 7). The trench-derived earthquake history has age data for all paleoearthquakes (Fig. 7) from abundant ^{14}C age determinations on charcoal in soils buried by earthquakes. In contrast, only the youngest earthquake recorded at the coast has an age (A.D. 900–930) derived from radiocarbon dating (Atwater, 1999). The next-to-youngest earthquake recorded by an uplifted shore platform is broadly constrained to be older than A.D. 900 but younger than ca. 6 ka, which is the time when global sea level rise decelerated and sea level stabilized so that coastal landforms such as wave-cut platforms could be formed and preserved (Stanley and Warne, 1994) (Fig. 7).

Three earthquakes, and possibly four, have occurred in the past 2500 yr based on comparing the number and timing of earthquakes recorded in trench CL on the Toe Jam Hill fault (see trench location, Fig. 4) with those recorded by the uplifted shore platforms (Fig. 7). The youngest earthquake, which is the A.D. 900–930 regional-uplift earthquake, is correlative to the 0.2–1.2 ka earthquake that caused up to 2 m of vertical displacement on the Toe Jam Hill fault in the middle of Bainbridge Island (Fig. 7). However, vertical displacement from the 0.2–1.2 ka earthquake was less than 1 m along strike to the east and west where the fault intersects the island's coast. The next-to-youngest earthquake, which was confined to the reverse fault and did not cause regional

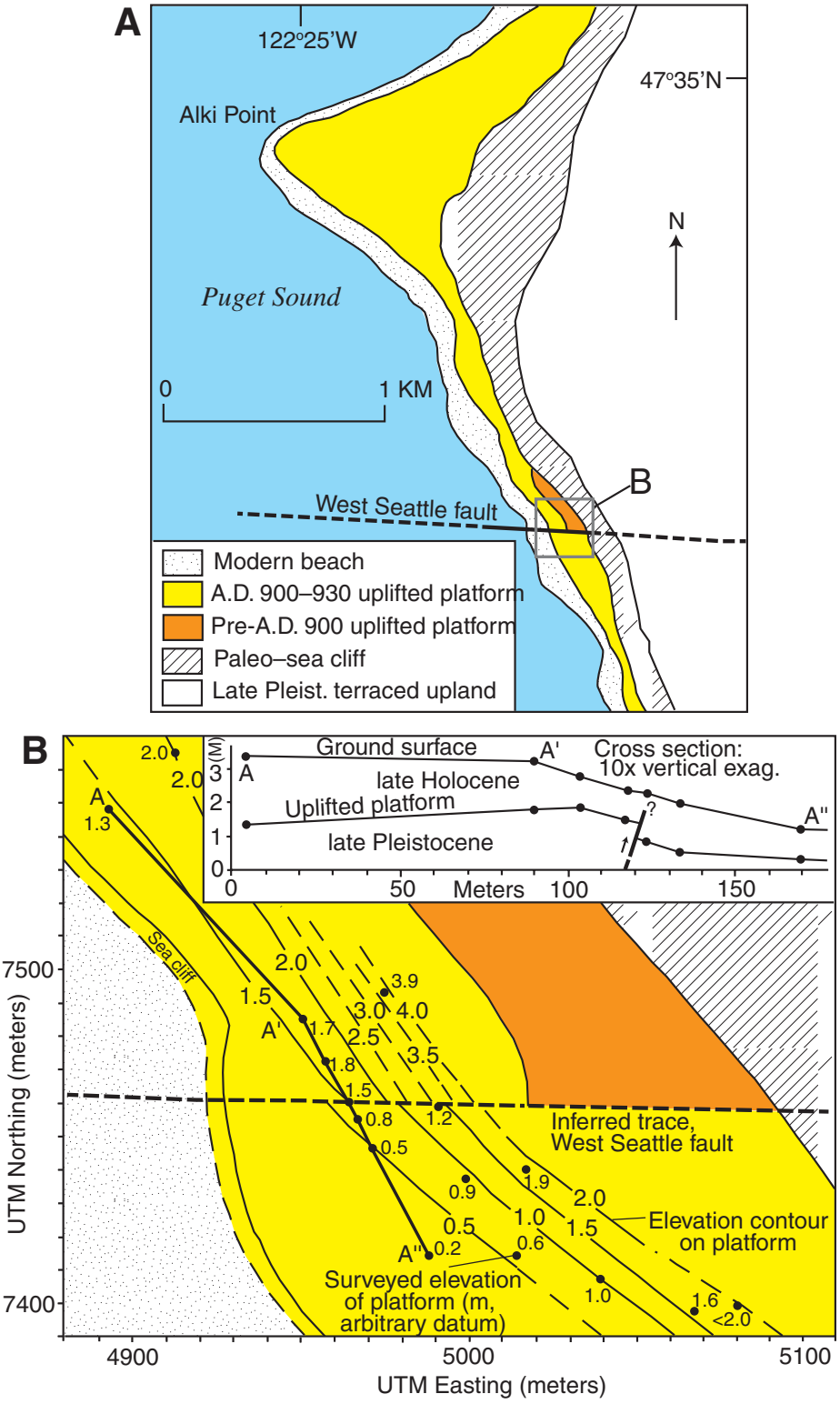

Figure 6. (A) Simplified map of the West Seattle area in the vicinity of Alki Point (map location on Fig. 1A) showing the West Seattle north-side-up reverse fault, the uplifted A.D. 900–930 platform, and the extent of the shore platform uplifted in a separate earthquake some time prior to A.D. 900–930. (B) Structure contour map, derived from auger data, of the uplifted A.D. 900–930 shore platform. Contour interval is 0.5 m. Cross-section A–A″ depicts the offset (~1.5–2.0 m up to the north) of the platform along Beach Drive. Structure contours indicate that the platform is offset across a width of <5 m. UTM—Universal Transverse Mercator.

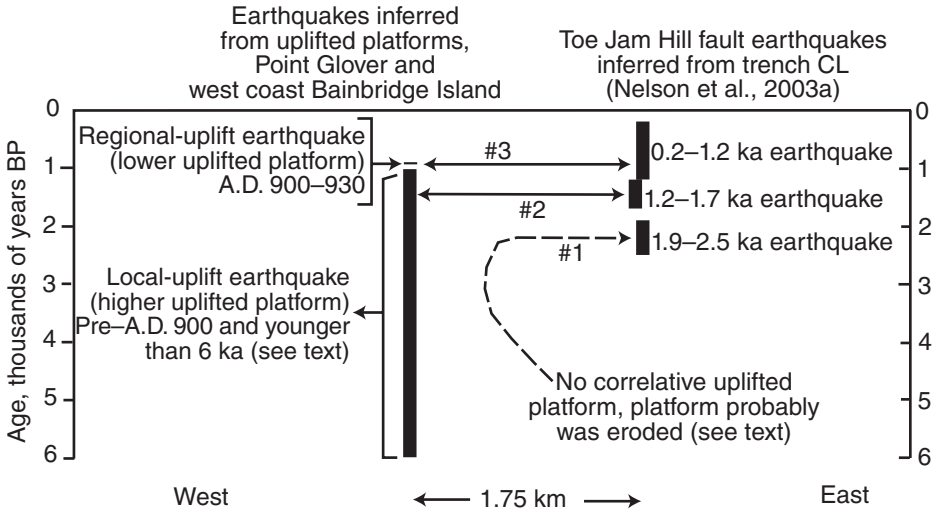

Figure 7. Space-time diagram for earthquakes recorded on shore platforms compared to earthquakes recorded in trench stratigraphy on the Toe Jam Hill fault (Nelson et al., 2003a). Ages are delineated by solid vertical bars. Ages of Toe Jam Hill fault earthquakes from Nelson et al. (2003a). Age of A.D. 900–930 regional uplift earthquake from Atwater (1999). The age of the local-uplift earthquake that uplifted the higher platform is pre–A.D. 900 but younger than mid-Holocene (see text). Horizontal arrow shafts correlate earthquakes recorded at coast (uplifted platforms) with earthquakes recorded inland (trenches).

uplift, uplifted shore platforms by ~3.5 m (Figs. 4 and 5) and probably is correlative with 1.2–1.7 ka earthquake recorded in trench CL on the Toe Jam Hill fault (Fig. 7). The oldest earthquake, which did not cause regional uplift, is recorded by the 1.9–2.5 ka north-side-up reverse fault earthquake on the Toe Jam Hill fault (Nelson et al., 2003a), but is not recorded by uplifted shore platforms (Fig. 7). The shore platform that was uplifted during the oldest earthquake is not preserved probably because the 1.9–2.5 ka uplift was small enough (<~2 m) that the uplifted platform was fully removed by sea cliff erosion before the next-to-youngest (1.2–1.7 ka) earthquake.

Four, rather than three, earthquakes since 2.5 ka occurred only if the A.D. 900–930 earthquake recorded at the coast is not the same earthquake as the 0.2–1.2 ka reverse fault earthquake recorded in trench CL. However, the timing of the youngest reverse fault earthquake (prehistoric but younger than 1.2 ka) overlaps in time the A.D. 900–930 earthquake (Fig. 7). Furthermore, nearby reverse faults did slip during the A.D. 900–930 regional uplift earthquake at both Waterman Point (Nelson et al., 2003b, 2003c) and at West Seattle. The Toe Jam Hill fault could have slipped at the time of the regional uplift as well. The most likely scenario, therefore, is three earthquakes since 2.5 ka in the Bainbridge Island and Point Glover areas with the most recent A.D. 900–930 earthquake, which is the regional-uplift earthquake, involving up to 2 m of vertical displacement on the Toe Jam Hill fault in the middle of the island but vertical displacements of less than 1 m along strike to the east and west at the coast.

In the Seattle fault zone, three north-side-up, bedding-plane reverse faults, the Toe Jam Hill fault on Bainbridge Island, the Point Glover fault at Point Glover, and the West Seattle fault near Alki Point (Figs. 1 and 6), slipped during earthquakes prior to the A.D. 900–930 regional-uplift earthquake. The uplift footprint for an earthquake associated with these reverse faults was locally confined to a limited area north of the fault (Figs. 4, 5, and 6). Of these three reverse faults, the Toe Jam Hill and Point Glover could behave as one fault segment (Fig. 8), but the West Seattle fault is less likely to be the same fault as the other two because the West Seattle fault is 8 km to the west-southwest and is not along strike (Fig. 1).

If the Toe Jam Hill and the Point Glover faults behave as one fault segment, then the next to oldest earthquake recorded by the higher uplifted platform on the west coast of Bainbridge Island (the 1.2–1.7 ka earthquake, Fig. 7) was also recorded by uplift of the higher platform at Point Glover (Fig. 7). The Toe Jam Hill fault and the Point Glover fault are almost along strike of each other, and they may be connected across the narrow 1.7-km–wide Rich Passage (Figs. 1B and 8). For the two faults to be connected, the connecting segment must have a slightly more northerly strike or there must be an ~250 m left step in the fault trace (Fig. 8). If connected, the 1.2–1.7 ka earthquake likely included slip on both the Toe Jam Hill and the Point Glover faults.

DISCUSSION

Can Bedding-Plane Faults Generate Earthquakes?

Bedding-plane slip at shallow to intermediate (3–12 km depth) levels is implicated for earthquakes in many convergent and obliquely convergent structural settings in addition to the Seattle fault zone (Philip and Meghraoui, 1983; Yeats, 1986; McInelly and Kelsey, 1990; Tsutsumi and Yeats, 1999; Guzofski et al., 2007). Bedding-plane faults have ruptured coseismically and produced surface scarps in conjunction with large earthquakes on deeper structures (Lensen and Otway, 1971; Philip and Meghraoui, 1983; Hull, 1990; Treiman, 1995; Yeats, 2000). While in some cases bedding-plane faults above thrust wedges and passive roof duplexes root in thrust ramps or roof thrusts (Banks and Warburton, 1986; Guzofski et al., 2007), in other cases bedding-plane reverse faults root in the axial plane region of folds (Shaw and Suppe, 1994; Ishiyama et al., 2004).

Folds can generate fault slip on bedding planes through the mechanism of flexural-slip (Yeats, 1986; Yeats et al., 1997); and based on geologic mapping supplemented by depth control from well logs, Yeats et al. (1981) contended that flexural-slip, bedding-plane faults can be seismogenic without being triggered by coseismic slip on deeper crustal faults. Adams (1984) made a similar case that bedding-plane faults rooted in a fold axis are seismogenic, while McInelly and Kelsey (1990) argued that these same bedding-plane faults probably are triggered by deeper crustal structures. As discussed above, Shaw and Suppe (1994) interpreted that bedding-plane surfaces in proximity to the active axial surface of a fault-bend fold in bedded sedimentary rocks in the Santa Barbara channel produced a swarm of $<M_L 4$ earthquakes, the hypocenters of which outline the active axial surface. In contrast, Nicholson et al. (2007) interpret the axial surface also to be a high-angle fault, in which case the earthquakes may have been produced on this fault. In either case, the axial surface roots in the underlying, active Channel Islands thrust ramp, and the earthquake swarm was not triggered by coseismic slip on the underlying thrust ramp. Other examples of bedding-plane fault earthquakes not linked to slip on crustal faults at deeper levels include earthquakes generated by removal of overburden in quarries that initiated small reverse fault earthquakes confined to

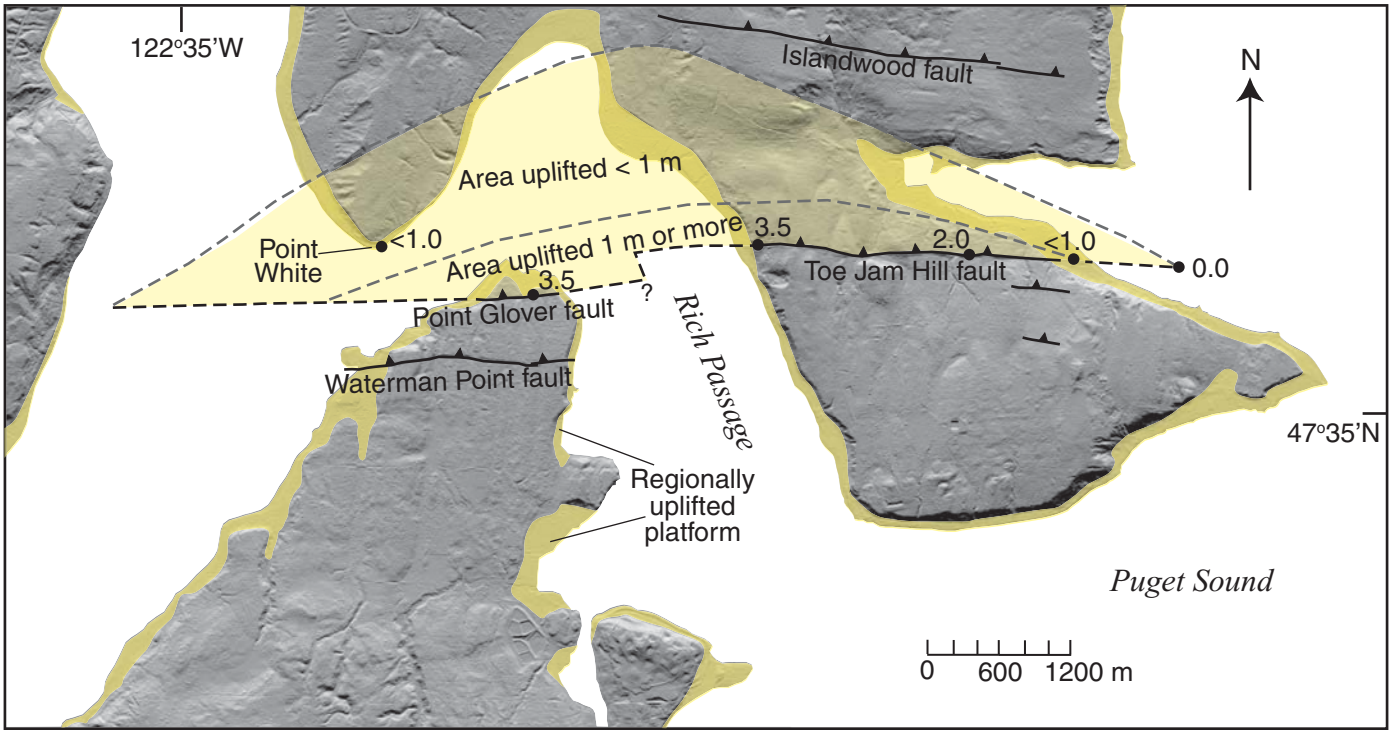

Figure 8. Light detection and ranging (LiDAR) image showing inferred rupture patch (yellow), projected to ground surface, from a bedding-plane reverse-fault earthquake (Toe Jam Hill/Point Glover earthquake) within the Seattle fault zone that probably occurred 1.2–1.7 ka (Fig. 7). The earthquake occurred on a ~60°–80° north-dipping fault. Numbers refer to amount of coseismic uplift. The inferred tear fault in Rich Passage is questioned because the Point Glover and Toe Jam Hill faults alternatively may connect by a curved fault trace.

bedding planes (Yerkes et al., 1983; Sylvester and Heinemann, 1996).

In the hanging wall north of bedding-plane–parallel reverse faults of the Seattle uplift, the limited spatial extent of coseismic uplift is best explained by earthquakes confined to the reverse faults. The earthquakes are projected to be 5.6–6.0 magnitude events (see below) which, although not large, present an appreciable seismic hazard because the earthquakes are probably shallow (~5 km depth) and the reverse fault traces trend across the greater Seattle metropolitan area.

Two Types of Earthquakes Inferred from Shore Platform Deformation

Paleoseismic evidence of earthquakes in the Seattle fault zone points to two different ground surface responses to two distinctly different paleoearthquakes. The first type of paleoearthquake, represented by the A.D. 900–930 earthquake, caused regional uplift across much of the ~6–7 km width of the Seattle fault zone. Brocher et al. (2004) suggest a passive roof duplex model for the A.D. 900–930 earthquake. Ten Brink et al. (2006) adopt the roof duplex model and, assuming that shore platforms over a 6-km width were coseismically uplifted 6–7 m, place constraints on the dip of the floor thrust (50°) and on the fault geometry. In the models of both Brocher et al. (2004) and ten Brink et al. (2006), the A.D. 900–930 earthquake ruptures the north-vergent floor thrust (the master-ramp thrust), the south-vergent roof thrust (a backthrust that roots in the master ramp), and some of the south-vergent, bedding-plane reverse faults above the roof thrust (Fig. 2B).

The second type of paleoearthquake, represented by the second-to-most recent earthquake on the Toe Jam Hill fault, involves slip of one or several bedding-plane reverse faults, generates surface faulting, and causes localized uplift hundreds of meters north of fault scarps but not regional uplift.

Some component of slip on bedding-plane faults may be aseismic, but field and seismic evidence suggests that bedding-plane slip is at least in part coseismic. Multiple-meter high fault scarps along the Waterman Point, Point Glover, and Toe Jam Hill faults (Nelson et al., 2003a, 2003b, 2003c), localized abrupt uplift of shore platforms adjacent to bedding-plane reverse faults, and the Point White earthquake (discussed below) are all observations that support coseismic slip on bedding planes in the Seattle fault zone during earthquakes that generate localized deformation but not regional uplift.

Revised Structural Model for the Seattle Fault Zone

We propose an alternative model for the Seattle fault zone (Fig. 9) that incorporates interpretations of Brocher et al. (2004) and ten Brink et al. (2006) with observations of the timing and extent of surface faulting from uplifted shorelines and paleoseismic studies. This model uses mapped surface traces of active reverse faults (Point Glover, Toe Jam Hill, and Islandwood) and evidence for late Holocene uplift associated with these faults to help define the geometry of the underlying wedge thrust and fault-bend fold.

We infer that the Seattle monocline is a doubly vergent wedge thrust fold (Medwedeff, 1992; Ishiyama et al., 2004) with the active axial surface of the fault-bend fold intersecting the ground at the surface transition from the Seattle basin to the Seattle uplift (A1 in Figs. 1A and 9B). The mapped scarps of the active reverse faults (Toe Jam Hill and Islandwood) help define where the active axial surface intersects the ground surface (Fig. 9B). The limb of the

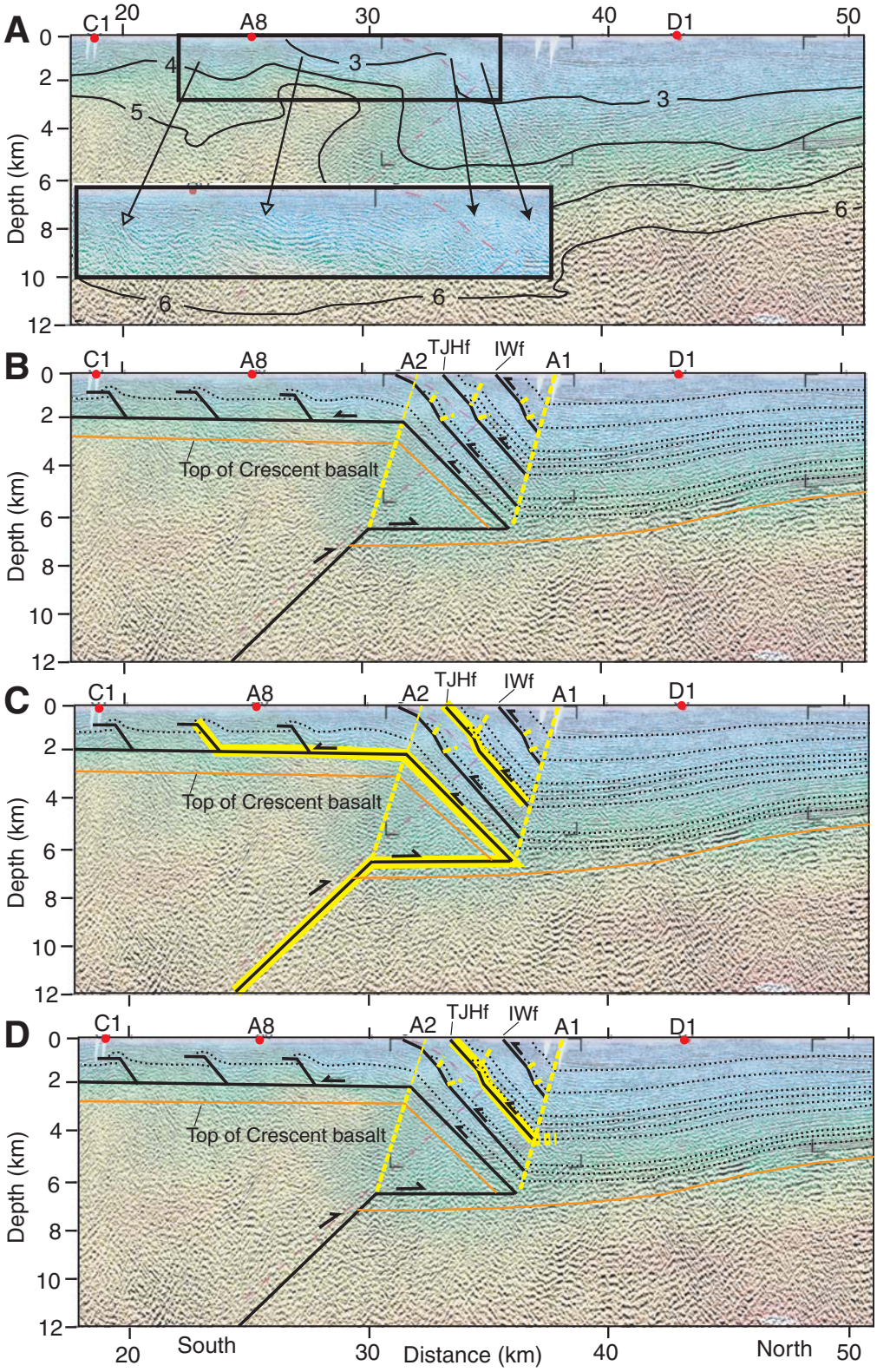

Figure 9. Schematic interpretation of proposed Seattle fault zone structural geometry. (A) P-wave–velocity model of Seismic Hazards Investigation in Puget Sound (SHIPS) seismic reflection line PS-2; C1, A8, and D1 are locations of seismometers along seismic line (see Fig. 1A); black lines, isovelocity contours at 1 km/sec intervals (ten Brink et al., 2002). Inset shows enlarged portion of seismic line in upper 3 km in vicinity of bedding-plane reverse faults. (B) Doubly vergent wedge thrust fold interpretation for the Seattle fault zone. Bold black lines—faults; dashed black lines—bedding; bold dashed yellow lines—active axial surfaces of fault-bend folds; thin dashed yellow lines—inactive axial surface; orange line—top of Eocene Crescent Formation basalt. Note the bedding-plane reverse faults root in the steeply dipping synclinal axial surface and not in the roof thrust, as originally proposed by Brocher et al. (2004) (Fig. 2C). (C) Inferred extent of slip (solid-yellow bold lines) for an earthquake causing regional coseismic uplift, such as occurred in A.D. 900–930. (D) Inferred extent of slip (yellow bold line) for an earthquake confined to bedding-plane reverse fault (a "folding earthquake"), which would generate a north-side-up fault scarp and localized uplift extending hundreds of meters north of the fault scarp. The dashed, bold-yellow "tail" of the inferred slip denotes that the slip may also occur north of the axial surface in the flat portion of the fault-bend fold. TJHf—Toe Jam Hill fault; IWf—Islandwood fault.

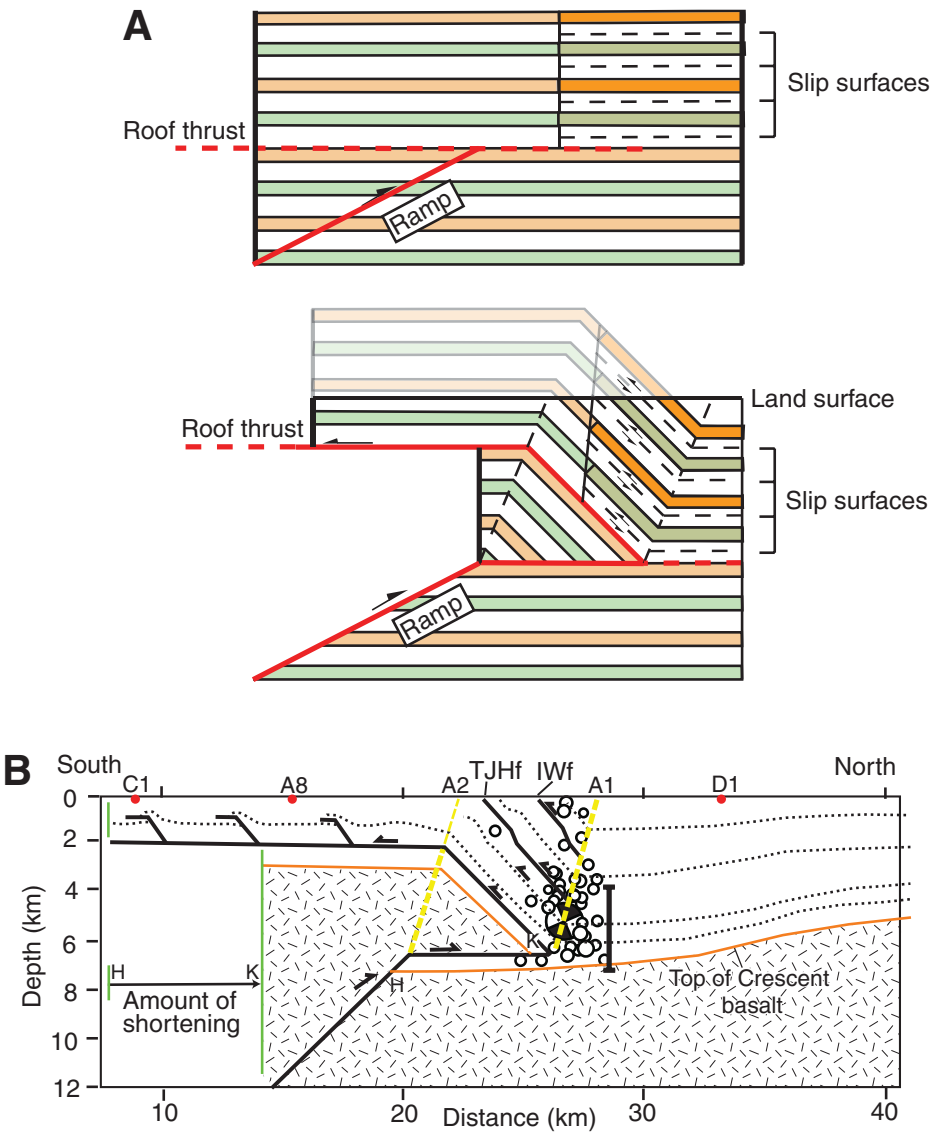

Figure 10. (A) Simple theoretical model, using fault-related folding theory (Suppe, 1983; Medwedeff, 1992), showing how bedding-plane reverse faults would grow as slip accumulates on the master ramp. The model demonstrates the permissible kinematic relationship between slip on bedding-plane reverse faults, which would produce localized uplift to the north of reverse fault scarps, and slip on the Seattle thrust ramp. Note that the inferred ramp angle for the Seattle fault zone (Figs. 9 and 10B), based on interpretation of the seismic reflection profile, and the ramp angle in the theoretical model are not the same because the theoretical model consists of a layered medium in both the hanging wall and footwall, whereas the massive, fractured Crescent basalt does not consist of layers that deform by layer parallel slip. (B) Wedge thrust fold model for the Seattle fault zone and focal mechanism for the 1997 Point White earthquake (beach ball) and aftershocks (open white circles) (Blakely et al., 2002). The solid vertical bar shows the depth uncertainty for the main shock (Pacific Northwest Seismic Network, 2007). The focal mechanism is projected 8 km west along strike from its epicentral location (Fig. 1A), using the position of the earthquake relative to the surface trend of axial plane A1. The amount of shortening is inferred from the kink band width from H to K. The cross section is line length balanced for the top of Crescent basalt (orange line) and the lowermost bed contact from seismic reflection line (dotted line). C1, A8, and D1 are seismometer locations on the seismic line in Figure 1A.

fold south of the active axial surface is the moderately to steeply dipping (60°–80°N) structural panel of Tertiary strata that contains bedding-plane–parallel reverse faults.

These reverse faults are bedding-plane thrusts that root in the active axial surface of the fold. This geometry allows for reverse slip on 60°–80° north-dipping bedding planes, as observed in trenches (Nelson et al., 2003a) (Fig. 2A). Based on dips of the reverse faults at the surface, and on the dips of sedimentary beds, the reverse faults are interpreted to root in the synclinal axial surface at depths of 4–6 km (Fig. 9). An earthquake confined to these steep bedding-plane faults would produce localized uplift to the north of north-side-up reverse fault scarps. A possible theoretical model (after Medwedeff, 1992) shows how such bedding-plane reverse faults would grow as slip accumulates on the master ramp (Fig. 10A). Bedding-plane slip accumulates as the forelimb of the structural wedge associated with the Seattle ramp widens. We interpret the forelimb of the wedge to be a fault-related fold that deforms by flexural slip processes (Yeats et al., 1997). The model in Figure 10 demonstrates the permissible kinematic relationship between bedding-plane reverse faults and slip on the Seattle thrust ramp as constrained by surface observations of bedding dip and reverse fault scarps and seismic reflection data.

We therefore envision the Seattle fault zone as a seismogenic structural wedge (Fig. 9), in contrast to prior interpretations of the Seattle fault as a reverse fault with a backthrust (ten Brink et al., 2002) or as a structural duplex (Brocher et al., 2004) (Fig. 2). A similar seismogenic structural wedge underlies Wheeler Ridge in the southern San Joaquin Valley (Medwedeff, 1992) and the Coyote Hills segment of the Puente Hills blind-thrust fault in the Los Angeles basin (Pratt et al., 2002). According to fault-bend fold theory (Suppe, 1983), the total shortening on the wedge thrust is equal to the 6-km width of the kink fold between the active axial surface A1 and the inactive axial surface A2 (Figs. 9 and 10B). If the total slip on the master-ramp thrust is ~6 km and the master ramp dips 40°–60° (ten Brink et al., 2006), the vertical offset of the Seattle basin from the Seattle uplift is 4.6–5.2 km, which is roughly the relief of the basin compared to the neighboring uplift (vertical offset of top of Crescent Formation, Fig. 9) as inferred from P-wave–velocity modeling (ten Brink et al., 2002). Minor folds in the sedimentary units, which often are associated with faults at the surface, are consistent with a fault ramp and bedding cutoff fold geometry. For instance, the seismic line shows minor folds in the steeply dipping bedded section below the reverse fault scarps (solid arrows point to such folds on inset to Fig. 9A). We infer that these folds are hanging-wall bedding cutoffs that are formed by fault ramps where the reverse faults cut obliquely up-section from one bedding plane to another. Similarly, farther south on the seismic line, folds in the upper few kilometers of the Tertiary bedded section perturb the otherwise shallow beds dips (open arrows point to such folds on inset to Fig. 9A). We infer these folds are also hanging-wall bedding cutoffs, in this case formed by fault ramps where reverse faults cut obliquely up-section from the underlying roof thrust.

The wedge thrust, fault-bend fold model can explicitly account for the two earthquake types identified by paleoseismology studies. Regional uplift earthquakes can accommodate, but do not require, slip on the bedding-plane reverse faults. The bold yellow lines in Figure 9C delineate faults that would rupture during a regional uplift earthquake. These faults include the master ramp and flat, the backthrust of the wedge, and the hinterland bedding-plane detachment ("roof thrust"); a regional uplift earthquake could also include slip on a bedding-plane–parallel reverse fault (Fig. 9C). Bedding-plane–parallel reverse fault earthquakes, which produce only localized uplift, can occur independently of slip on the master ramp and wedge thrust. The bold yellow line in Figure 9D schematically delineates a fault that could rupture during an earthquake confined to a bedding-plane–parallel reverse fault rooted in the active axial surface.

The June 23, 1997, M_w4.5 Point White earthquake (Pacific Northwest Seismic Network, 2007) is an earthquake within the Seattle fault zone (Fig. 1A) that likely initiated by slip on bedding planes within or near the active synclinal axial surface above the structural wedge of the Seattle fault zone. The focal mechanism and depth, if plotted 8 km eastward along strike onto the line of the seismic section, shows that the reverse focal mechanism occurred at a shallow depth (4.0–8.0 km, Pacific Northwest Seismic Network, 2007) with a hypocentral position within steeply dipping bedded sediment at the north end of the Seattle uplift (Fig. 10B). The depth and position of the focal mechanism are consistent with earthquake initiation by slip on bedding planes near the axial surface of the Seattle monocline (A1, Fig. 10B). The two possible slip planes for the earthquake have strikes parallel to the regional strike of the Tertiary strata (090°) and one of the planes dips 65° to 85°N (Pacific Northwest Seismic Network, 2007), which is the same as the local dip of the Tertiary strata (Figs. 1B and 10B). We infer that the Point White earthquake is similar to the localized-uplift earthquakes inferred from platform uplift at Bainbridge Island and Point Glover (Figs. 4 and 5) except that the Point White earthquake was too small to generate a surface scarp or to preserve shore platform uplift.

The Late Holocene Toe Jam Hill/Point Glover Bedding-Plane Reverse Fault Earthquake

At least two earthquakes that involved slip on the Toe Jam Hill fault occurred hundreds to a few thousand years prior to the A.D. 900–930 regional uplift earthquake (Nelson et al., 2003a; Fig. 7), and in this section we reconstruct the likely rupture area of one of those earthquakes, herein called the Toe Jam Hill/Point Glover earthquake (earthquake #2 in Fig. 7). The earthquake ruptured the Toe Jam Hill and Point Glover north-side-up, bedding-plane reverse faults, which we infer to be connected across Rich Passage (Fig. 8). Although in this reconstruction we restrict the earthquake rupture area to these two faults, we recognize that other separate bedding-plane reverse faults, such as the Waterman Point fault, the Islandwood fault, and/or the West Seattle fault (Fig. 1), could have ruptured in earthquakes at the same time, producing other areas of localized surface uplift.

We approximate the extent and amount of the surface coseismic uplift from the Toe Jam Hill/Point Glover earthquake (Fig. 8) by compiling coseismic uplift estimates from trench investigations (Nelson et al. 2003a) and from wave-cut platform studies discussed above. Uplift on the fault trace at Point Glover and on the west coast of Bainbridge Island was ~3.5 m (Figs. 4 and 5), and uplift on the Toe Jam Hill fault in the middle of Bainbridge Island at the site of trench excavations was 2.0 m (Nelson et al., 2003a). Evidence for a higher shore platform above the A.D. 900–930 regionally uplifted platform is lacking both at Point White and on the east coast of Bainbridge Island, and therefore uplift at these sites probably was less than one meter (Fig. 8). Because coseismic surface uplift decreases to the east and to the west from a maximum between Point Glover and the west coast of Bainbridge Island, we approximate eastern and western limits to surface rupture, which define an ~8- to 10-km–long fault trace (a ~9-km–long trace is depicted in Fig. 8). Although the maximum slip is on the order of 3.5–4.0 m (Figs. 4 and 5), much of the area was coseismically uplifted less than one meter (Fig. 8); thus, we assign a conservative average slip of 2 m. Subsurface geometry based on seismic reflection data (Figs. 2 and 9) suggests that the bedding-plane faults root at 4–6 km depth, possibly in the vicinity of the axial surface of the fault-bend fold.

Fault rupture characteristics for the Toe Jam Hill/Point Glover earthquake (rupture plane that

is 8–10 km long and 4–6 km deep with an average fault slip of 2 m) would generate an earthquake of moment magnitude 5.6–6.0, using a material shear modulus range for sedimentary rocks of 0.5×10^{11} GPa to 0.9×10^{11} GPa (Brocher, 2005) and the moment magnitude relation developed by Hanks and Kanamori (1979). An example of a historic reverse fault earthquake with similar surface scarp length, vertical displacement, and epicentral depth to the reconstructed Toe Jam Hill/Point Glover earthquake, but hosted in rocks with higher shear moduli, is the 1988 Tennant Creek (Australia) earthquake sequence (Crone et al., 1992). These three M_S 6.3–6.7 reverse fault earthquakes had surface fault scarp lengths of 3.1–16.0 km, vertical displacements of 1.0–1.5 m and main shock depths of 3.5–6.5 km. In general, the reverse fault earthquake depicted in Figure 8 has a short rupture length for the average amount of slip compared to historic earthquakes generated by reverse faults (Wells and Coppersmith, 1994). The 1983 M_W 6.5 Coalinga earthquake, for instance, had maximum surface uplift of 0.5 m from a combined rupture length of 20–35 km with primary and secondary slip on several shallow (<30°) ramp thrusts and bedding-plane reverse faults above a 10 km main shock depth (Eaton, 1990; Stein and Ekström, 1992). However, the maximum surface uplift was not on a fault scarp but occurred directly above an actively growing fault-bend fold at depth, where no bedding-plane reverse faults were observed at the surface (Guzofski et al., 2007).

Timing of Folding Earthquakes Relative to Timing of Master-Ramp Earthquakes

Earthquakes generated in the axial plane region of a fault-bend fold ("folding earthquakes") are, in the broadest sense, kinematically driven by earthquakes on the master ramp because coseismic slip on the master ramp results in growth of the fault-bend fold in the overlying sedimentary basin at the tip of the wedge thrust. If slip occurs on flexural slip bedding-plane surfaces of a fault-bend fold during a master-ramp earthquake, then there is no folding earthquake separated in time from the master-ramp earthquake, although reverse fault scarps generated by bedding-plane slip may be preserved at Earth's surface. However, if bedding-plane slip is delayed by hours to years, a separate folding earthquake (i.e., seismic slip on bedding planes) would occur. The folding earthquake must occur centuries after the master-ramp earthquake in order for the uplift from the folding earthquake to be recorded by a separate uplifted shore platform.

Timing of Seattle fault zone earthquakes (Sherrod et al., 2000; Nelson et al., 2003a; 2003b) may provide insight to the time range of triggering of folding earthquakes by master-ramp earthquakes. The earthquake record comes from several sources, the best documented of which are the 7500 yr continuous relative sea-level stratigraphic record from the marsh at Restoration Point (Sherrod et al., 2000) (Fig. 1) and the late Holocene paleoseismic record from the Waterman Point and Bainbridge Island trench investigations (Nelson et al., 2003a, 2003b, 2003c).

The Holocene record of earthquakes on the Seattle fault zone (Fig. 11) indicates that folding earthquakes can be triggered from hours to thousands of years after the last master-ramp earthquake. A large earthquake 7000 yr ago produced regional uplift (Sherrod et al., 2000) and was followed by a ~4500 yr time gap before a cluster of ~2–3 folding earthquakes. This cluster of folding earthquakes was immediately followed by the A.D. 900–930 regional-uplift, master-ramp earthquake (Fig. 11). The A.D. 900–930 regional-uplift earthquake included slip on bedding-plane reverse faults that formed scarps at the surface. Although folding earthquakes are considered to be kinematically induced by deeper-seated master-ramp earthquakes, their timing can be sufficiently delayed relative to the preceding master-ramp earthquake to appear as a precursory event for the next master-ramp earthquake in the paleoseismic record (Fig. 11). Such is the case in the Seattle fault zone where some

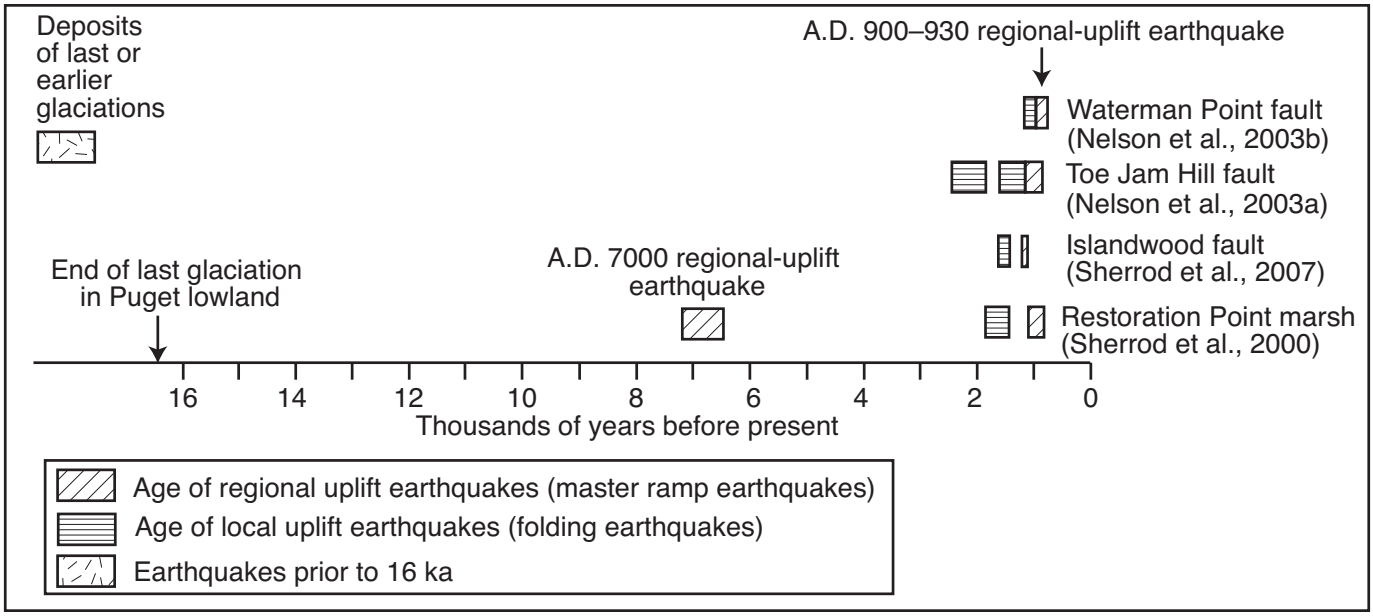

Figure 11. Summary of earthquake timing from trench (Nelson et al., 2003a, 2003b; Sherrod et al., 2007), shore platform (this study), and marsh (Sherrod et al., 2000) investigations within the Seattle fault zone. All locations are depicted on Figure 1B. The age range denoted by the bar widths is the maximum limiting age for the earthquake based on radiocarbon ages on detrital charcoal. Earthquakes in the paleoseismic record of the Seattle fault zone are divided into three categories (regional, local, and older than 16 k.y.) based on age and extent of shoreline uplift associated with the earthquake

folding earthquakes occur thousands of years after the master-ramp earthquake. The folding earthquakes of 1.2–1.7 ka and 1.9–2.5 ka (Figs. 7 and 11) were precursors to the A.D. 900–930 regional-uplift, master-ramp earthquake.

But the Seattle fault zone paleoseismic data also allow that folding earthquakes may be triggered within hours to months after the master-ramp earthquake. At the West Seattle and Waterman Point sites (Figs. 5 and 6), we have inferred that the Waterman Point reverse fault and the West Seattle reverse fault slipped at the same time as the A.D. 930–900 master-ramp earthquake, but these bedding-plane faulting events may have occurred days to months after the A.D. 930–900 master-ramp earthquake and the record of a regionally uplifted platform locally offset by a reverse fault scarp would be preserved the same either way.

CONCLUSIONS

Folding earthquakes, generated in the axial plane region of fault-bend folds, can be independent seismic hazards. These earthquakes involve coseismic fold growth as part of the deformation field of the earthquake and are distinct from earthquakes that occur on master-ramp thrusts.

The Seattle fault zone consists of a blind north-verging wedge thrust that poses a considerable seismic hazard to the Seattle metropolitan region from two seismogenic sources. One earthquake source is the master-ramp thrust and associated backthrust and roof ramp of the wedge thrust. Such earthquakes generate regional uplift along the ~6- to 7-km–wide Seattle uplift; and the hazard of such an earthquake, which last occurred in A.D. 900–930, has been identified by other workers. The other earthquake source is relatively shallow (<6-km–deep) faults that occur on flexural slip surfaces within the fault-bend fold at the tip of the thrust wedge. These bedding-plane faults slip coseismically during folding. The folding earthquakes, generated in the axial region of the fold, propagate up steep bedding dips to form the observed north-side-up fault scarps in the Seattle fault zone. Evidence for these folding earthquakes comes from uplifted shore platforms formed on the north side of uplifted bedding-plane reverse fault scarps. Such uplifted platforms only extend hundreds of meters north of the fault scarps and are distinctly restricted in areal extent compared to the regionally extensive uplifted shore platform (6–7 km wide, ~25 km along strike) that is the result of a wedge thrust earthquake. Nonetheless, the folding earthquakes present a significant, separate seismic hazard. Folding earthquakes are probably in the range of magnitude 6, based on estimated slip amounts and rupture area on flexural slip surfaces for one folding earthquake reconstructed from paleogeodetic data derived from uplifted shore platforms.

A conceptual model of the Seattle fault zone as a doubly vergent wedge thrust fold not only provides a structural context for reverse faults and folding earthquakes but also provides insight to Seattle basin development. The width of the kink of the fault-bend fold at the tip of the Seattle fault zone wedge thrust is 6 km, which, following fault-bend fold theory, would predict that total slip on the wedge thrust is 6 km. Given a 50°–60° dip of the master ramp, the wedge thrust would create a basin ~4–6 km deep, a depth consistent with that of the Seattle basin in the foreland of the wedge thrust.

In the Holocene, folding earthquakes on the Seattle fault zone have occurred thousands of years after the previous master-ramp earthquake. Folding earthquakes in the broadest sense are triggered by earthquakes on the master ramp because coseismic slip on the master ramp results in growth of the fault-bend fold at the tip of the wedge thrust. If slip occurs on flexural slip bedding-plane surfaces in the fault-bend fold during the master-ramp earthquake, then there is no separate folding earthquake. However, if slip is delayed by hours to years, a separate folding earthquake would occur. Based on an earthquake history record for the Seattle fault zone that spans the past 7500 yr, folding earthquakes can be triggered from hours to thousands of years after the last master-ramp earthquake, and some folding earthquakes may be precursory to the subsequent master-ramp earthquake.

ACKNOWLEDGMENTS

Research was funded by both the internal and external National Earthquake Hazards Reduction Program (NEHRP), external program award number 04HQGR0118. We gratefully acknowledge those who allowed us access to their coastal properties: Jim and Kristi O'Connor, Tom the carpenter (Bainbridge Island); Ernie Nagli, Bill Menees, Fred Cook, and Bud and Judy Myler (Point Glover). E. Barnett assisted with field work on Bainbridge Island, and the manuscript benefited from discussion with S. Cashman, J. Muller, and D. Harding. Reviews provided by S.M. Cashman, P. Eichhubl, C. Guzofski, K. Mueller, J. H. Shaw, U. ten Brink, and R.S. Yeats substantially improved the manuscript. C. Guzofski provided substantial insight to fault-bend folds.

REFERENCES CITED

Adams, J., 1984, Active deformation of the Pacific Northwest continental margin: Tectonics, v. 3, p. 449–472.

Atwater, B.F., 1999, Radiocarbon dating of a Seattle earthquake to A.D. 900–930: Seismological Research Letters, v. 10, p. 232.

Atwater, B.F., and Moore, A.L., 1992, A tsunami about 1,000 years ago in Puget Sound, Washington: Science, v. 258, p. 1614–1617, doi: 10.1126/science.258.5088.1614.

Banks, C.J., and Warburton, J., 1986, 'Passive roof' duplex geometry in the frontal structure of the Kirthar and Sulaiman mountain belts, Pakistan: Journal of Structural Geology, v. 8, p. 229–237, doi: 10.1016/0191-8141(86)90045-3.

Blakely, R.J., Wells, R.E., Weaver, C.S., and Johnson, S.Y., 2002, Location, structure and seismicity of the Seattle fault zone, Washington: Evidence from aeromagnetic anomalies, geologic mapping and seismic reflection data: Geological Society of America Bulletin, v. 114, p. 169–177, doi: 10.1130/0016-7606(2002)114<0169:LSASOT>2.0.CO;2.

Brocher, T.M., 2005, Empirical relations between elastic wave speeds and density in the Earth's crust: Bulletin of the Seismological Society of America, v. 95, p. 2081–2092, doi: 10.1785/0120050077.

Brocher, T.M., Blakely, R.J., and Wells, R.E., 2004, Interpretation of the Seattle uplift, Washington, as a passive-roof duplex: Bulletin of the Seismological Society of America, v. 94, p. 1379–1401, doi: 10.1785/012003190.

Bucknam, R.C., Hemphill-Haley, E., and Leopold, E.B., 1992, Abrupt uplift within the past 1700 years at southern Puget Sound, Washington: Science, v. 258, p. 1611–1614, doi: 10.1126/science.258.5088.1611.

Chen, Y.-G., Lai, K.-Y., Lee, Y.-H., Suppe, J., Chen, Y.-S., Lin, Y.-N.N., Wang, Y., Hung, J.-H., and Kuo, Y.-T., 2007, Coseismic fold scarps and their kinematic behavior in the 1999 Chi-Chi earthquake Taiwan: Journal of Geophysical Research, v. 112, B03S02, doi: 10.1029/2006JB004388

Crone, A.J., Machette, M.N., and Bowman, J.R., 1992, Geologic investigations of the 1988 Tennant Creek, Australia, earthquakes—Implications for paleoseismicity in stable continental regions: U.S. Geological Survey Bulletin 2032-A, 51 p.

Dolan, J.F., Christofferson, S.A., and Shaw, J.H., 2003, Recognition off paleoearthquakes on the Puente Hills blind thrust fault, California: Science, v. 300, p. 115–118, doi: 10.1126/science.1080593.

Eaton, J.P., 1990, The earthquake and its aftershocks from May 2 through September 30, 1983, in the Coalinga, California earthquake of May 2, 1983, edited by Rymer, M., and Ellsworth, W.: U.S. Geological Survey Professional Paper 1487, p. 113–170.

Fulmer, C.V., 1975, Stratigraphy and paleontology of the type Blakeley and Blakely Harbor Formation, *in* Weaver, D.W., Hornaday, G.R., and Tipton, A., eds., Conference on future energy levels of the Pacific coast, Paleogene symposium and selected technical papers: Long Beach, California, Fiftieth annual meeting of the American Association of Petroleum Geologists, SEPM (Society for Sedimentary Geology), and Society of Exploration Geophysicists, p. 210–271.

Guzofski, C.A., Shaw, J.H., Lin, G., and Shearer, P.M., 2007, Seismically active wedge structure beneath the Coalinga anticline, San Joaquin basin, California: Journal of Geophysical Research, v. 112, B03S05, doi: 10.1029/2006JB004465

Hanks, T.C., and Kanamori, H., 1979, A moment magnitude scale: Journal of Geophysical Research, v. 84, p. 2348–2350.

Harding, D.J., 2002, Folding and rupture of an uplifted Holocene marine platform in the Seattle fault zone, Washington, revealed by Airborne Laser Swath mapping: Geological Society of America Abstracts with Programs, v. 34, p. A-107.

Haugerud, R.A., Harding, D.J., Johnson, S.Y., Harless, J., Weaver, C.S., and Sherrod, B.L., 2003, High resolution lidar topography of the Puget Lowland, Washington: GSA Today, v. 13, p. 4–9, doi: 10.1130/1052-5173(2003)13<0004:HLTOTP>2.0.CO;2.

Henyey, T.L., and Teng, T., 1985, Seismic studies of the Dos Cuadras and Beta offshore oil fields, southern California OCS: Los Angeles, California, A final technical report submitted to the Department of the Interior, Minerals Management Service, by the Center for Earth Sciences, University of Southern California, Center for Earth Sciences, University of California, 40 p.

Hull, A.G., 1987, A late Holocene marine terrace on the Kidnappers Coast, North Island, New Zealand: Some implications for shore platform development processes and uplift mechanism: Quaternary Research, v. 28, p. 183–195, doi: 10.1016/0033-5894(87)90058-5.

Hull, A.G., 1990, Tectonics of the 1931 Hawke's Bay earthquake: New Zealand Journal of Geology and Geophysics, v. 33, p. 309–320.

Ishiyama, T., Mueller, K., Masami, T., Okada, A., and Keiji, T., 2004, Geomorphology, kinematic history, and earthquake behavior of the active Kuwana wedge thrust anticline, central Japan: Journal of Geophysical Research, v. 109, p. B12408, doi: 10.1029/2003JB002547

Johnson, S.Y., Dadisman, S.V., Childs, J.R., and Stanley, W.D., 1999, Active tectonics of the Seattle fault and central Puget Sound, Washington—Implications for earthquake hazards: Geological Society of America Bulletin, v. 111, p. 1042–1053, doi: 10.1130/0016-7606(1999)111<1042:ATOTSF>2.3.CO;2.

Lensen, G.J., and Otway, P.M., 1971, Earthshift and post-earthshift deformation associated with the May 1968 Inangahua earthquake, New Zealand: Royal Society of New Zealand Bulletin, v. 9, p. 107–119.

Marshak, S., and Mitra, G., 1988 Basic Methods of Structural Geology: Englewood Cliffs, New Jersey, Prentice Hall, 446 p.

McCaffrey, R., Long, M.D., Goldfinger, C., Zwick, P.C., Nabalek, J.L., Johnson, C.K., and Smith, C., 2000, Rotation and plate locking at the southern Cascadia subduction zone: Geophysical Research Letters, v. 27, p. 3117–3120, doi: 10.1029/2000GL011768.

McInelly, G.W., and Kelsey, H.M., 1990, Late Quaternary tectonic deformation in the Cape Arago-Bandon region of coastal Oregon as deduced from wave-cut platforms: Journal of Geophysical Research, v. 95, p. 6699–6713.

McLean, H., 1977, Lithofacies of the Blakeley Formation, Kitsap County, Washington: A submarine fan complex?: Journal of Sedimentary Research, v. 47, p. 78–88, doi: 10.1306/212F70F9-2B24-11D7-8648000102C1865D.

Medwedeff, D.A., 1992, Geometry and kinematics of an active, laterally propagating wedge thrust, Wheeler Ridge, California, *in* Mitra, S. and Fisher, G.W., eds., Structural geology of fold and thrust belts: Baltimore, Johns Hopkins University Press, p. 3–28.

Nelson, A.R., Johnson, S.Y., Kelsey, H.M., Wells, R.E., Sherrod, B.L., Pezzopane, S.K., Bradley, L., Koehler, R.D., and Bucknam, R.C., 2003a, Late Holocene earthquakes on the Toe Jam Hill fault, Seattle fault zone, Bainbridge Island, Washington: Geological Society of America Bulletin, v. 115, p. 1388–1403, doi: 10.1130/B25262.1.

Nelson, A.R., Johnson, S.Y., Kelsey, H.M., Sherrod, B.L., Wells, R.E., Okumura, K., Bradley, L., Bogar, R., and Personius, S.F., 2003b, Field and laboratory data from an earthquake history study of the Waterman Point fault, Kitsap County, Washington: U.S. Geological Survey Miscellaneous Field Studies Map MF-2423, http://pubs.usgs.gov/mf/2003/mf-2423/.

Nelson, A.R., Johnson, S.Y., Kelsey, H.M., Sherrod, B.L., Wells, R.E., Personius, S.F., Okumura, K., Bradley, L., and Bogar, R., 2003c, Late Holocene earthquakes on the Waterman Point reverse fault, another ALSM-discovered fault scarp in the Seattle fault zone, Puget lowland, Washington: Geological Society of America Abstracts with Programs, v. 35, p. 7.

Nicholson, C., Kamerling, M.J., Sorlien, C.C., Hopps, T.E., and Gratier, J.-P., 2007, Subsidence, compaction and gravity-sliding: Implications for 3D geometry, dynamic rupture and seismic hazard of active basin-bounding faults in southern California: Bulletin of the Seismological Society of America, v. 97, p. 1607–1620, doi: 10.1785/0120060236.

Pacific Northwest Seismic Network, 2007, Point White earthquake data, http://www.pnsn.org/SEIS/EQ_Special/WEBDIR_97062319131p/welcome.html

Philip, H., and Meghraoui, M., 1983, Structural analysis and interpretation of the surface deformations of the El Asnam earthquake of October 10, 1980: Tectonics, v. 2, p. 17–50.

Pratt, T.L., Johnson, S., Potter, P., Stephenson, W., and Finn, C., 1997, Seismic reflection images beneath Puget Sound: The Puget Lowland thrust sheet hypothesis: Journal of Geophysical Research, v. 102, p. 27,469–27,489, doi: 10.1029/97JB01830.

Pratt, T.L., Shaw, J.H., Dolan, J.F., Christofferson, S.A., Williams, R.A., Odum, J.K., and Plesch, A., 2002, Shallow seismic imaging of folds above the Puente Hills blind-thrust fault, Los Angeles, California: Geophysical Research Letters, v. 29, 1304, doi: 10.1029/2001GL014313

Shaw, J.H., and Suppe, J., 1994, Active faulting and growth folding in the eastern Santa Barbara channel, California: Geological Society of America Bulletin, v. 106, p. 607–626, doi: 10.1130/0016-7606(1994)106<0607:AFAGFI>2.3.CO;2.

Sherrod, B.L., Bucknam, R.C., and Leopold, E.B., 2000, Holocene relative sea level changes along the Seattle fault at Restoration Point, Washington: Quaternary Research, v. 54, p. 384–393, doi: 10.1006/qres.2000.2180.

Sherrod, B.L., Barnett, E.A., and Kelsey, H.M., 2007, An excavation log across an active strand of the Seattle fault zone: U.S. Geological Survey Open-File Report.

Stanley, D.J., and Warne, A.G., 1994, Worldwide initiation of Holocene marine deltas by deceleration of sea level rise: Science, v. 265, p. 228–231, doi: 10.1126/science.265.5169.228.

Stein, R.S., and Ekström, G., 1992, Seismicity and geometry of a 110-km long blind thrust fault: 2. Synthesis of the 1982–1985 California earthquake sequence: Journal of Geophysical Research, v. 97, p. 4865–4883.

Stein, R.S., and King, G.C.P., 1984, Seismic potential revealed by surface folding: 1983 Coalinga, California, earthquake: Science, v. 224, p. 869–872.

Suppe, J., 1983, Geometry and kinematics of fault-bend folding: American Journal of Science, v. 283, p. 684–721.

Sylvester, A.G., and Heinemann, J., 1996, Preseismic tilt and triggered reverse faulting due to unloading in a diatomite quarry near Lompoc, California: Seismological Research Letters, v. 67, p. 11–18.

ten Brink, U.S., Molzer, P.C., Fisher, M.A., Blakely, R.J., Bucknam, R.C., Parsons, T., Crosson, R.S., and Creager, K.C., 2002, Subsurface geometry and evolution of the Seattle fault zone and the Seattle basin, Washington: Bulletin of the Seismological Society of America, v. 92, p. 1737–1753, doi: 10.1785/0120010229.

ten Brink, U.S., Song, J., and Bucknam, R.C., 2006, Rupture models for the A.D. 900–930 Seattle fault earthquake from uplifted shorelines: Geology, v. 34, p. 585–588, doi: 10.1130/G22173.1

Treiman, J.A., 1995, Surface faulting near Santa Clarita, *in* Woods M.C., and Seiple, W.R., eds., The Northridge, California, earthquake of 17 January 1994: California Department of Conservation, Division of Mines and Geology Special Publication 116, p. 103–110.

Tsutsumi, H., and Yeats, R.S., 1999, Tectonic setting of the 1971 Sylmar and 1994 Northridge earthquakes in the San Fernando Valley, California: Bulletin of the Seismological Society of America, v. 89, p. 1232–1249.

Wells, D.L., and Coppersmith, K.J., 1994, New empirical relations among magnitude, rupture length, rupture width, rupture area and surface displacement: Bulletin of the Seismological Society of America, v. 84, p. 974–1002.

Wells, R.E., Weaver, C.S., and Blakely, R.J., 1998, Forearc migration in Cascadia and its neotectonic significance: Geology, v. 26, p. 759–762, doi: 10.1130/0091-7613(1998)026<0759:FAMICA>2.3.CO;2.

Wentworth, C.M. and Zoback, M.D., 1990, Structure of the Coalinga region and thrust origin of the earthquake, *in* Rymer, M.J., and Ellsworth, W.L., eds., The Coalinga, California, earthquake of May 2, 1983: U.S. Geological Survey Professional Paper 1487, p. 41–68.

Yeats, R.S., 1986, Active faults related to folding, *in* Active tectonics, p. 80–94: Washington, D.C., National Academy Press, 266 p.

Yeats, R.S., 2000, The 1968 Inangahua, New Zealand, and 1994 Northridge, California earthquakes: Implications for northwest Nelson: New Zealand Journal of Geology and Geophysics, v. 43, p. 587–599.

Yeats, R.S., Clark, M.N., Keller, E.A., and Rockwell, T.K., 1981, Active fault hazard in southern California: Ground rupture versus seismic shaking: Geological Society of America Bulletin, v. 92, p. 189–196, doi: 10.1130/0016-7606(1981)92<189:AFHISC>2.0.CO;2.

Yeats, R.S., Sieh, K., and Allen, C.R., 1997, The geology of earthquakes: New York, Oxford University Press, 568 p.

Yerkes, R.F., Ellsworth, W.L., and Tinsley, J.C., 1983, Triggered reverse fault and earthquake due to crustal unloading, northwest Transverse Ranges, California: Geology, v. 11, p. 287–291, doi: 10.1130/0091-7613(1983)11<287:TRFAED>2.0.CO;2.

Manuscript received 25 June 2007
Revised manuscript received 18 January 2008
Manuscript accepted 22 January 2008

Printed in the USA